nature communications

Article

https://doi.org/10.1038/s41467-025-59338-5

TRIM23 mediates cGAS-induced autophagy in anti-HSV defense

Received: 16 July 2024

Accepted: 16 April 2025

Published online: 13 May 2025

Check for updates

Dhiraj Acharya[1,2,11], Zuberwasim Sayyad[1,11], Helene Hoenigsperger[3], Maximilian Hirschenberger[3], Matthew Zurenski[2], Kannan Balakrishnan[1], Junji Zhu[1], Sebastian Gableske[2,10], Jiro Kato[4], Shen-Ying Zhang[5,6,7], Jean-Laurent Casanova[5,6,7,8], Joel Moss[4], Konstantin M. J. Sparrer[3,9] & Michaela U. Gack[1,2]

The cGAS-STING pathway, well-known to elicit interferon (IFN) responses, is also a key inducer of autophagy upon virus infection or other stimuli. Whereas the mediators for cGAS-induced IFN responses are well characterized, much less is known about how cGAS elicits autophagy. Here, we report that TRIM23, a unique TRIM protein harboring both ubiquitin E3 ligase and GTPase activity, is crucial for cGAS-STING-dependent antiviral autophagy. Genetic ablation of *TRIM23* impairs autophagic control of HSV-1 infection. HSV-1 infection or cGAS-STING stimulation induces TBK1-mediated TRIM23 phosphorylation at S39, which triggers TRIM23 autoubiquitination and GTPase activity and ultimately elicits autophagy. Fibroblasts from a patient with herpes simplex encephalitis heterozygous for a dominant-negative, kinase-inactivating *TBK1* mutation fail to activate autophagy by TRIM23 and cGAS-STING. Our results thus identify the cGAS-STING-TBK1-TRIM23 axis as a key autophagy defense pathway and may stimulate new therapeutic interventions for viral or inflammatory diseases.

Autophagy is a degradative pathway that, besides its well-characterized role in regulating energy homeostasis, orchestrates a variety of host-cell intrinsic and immune defenses[1–3]. Autophagy can degrade viral components leading to direct virus restriction or regulate pattern-recognition receptor (PRR)-mediated sensing or signaling[2,4] to influence virus-induced type I interferon (IFN) and inflammatory responses. Conversely, several PRRs that are well known to elicit antiviral cytokine induction also orchestrate autophagic responses. Notable among these PRRs is the DNA sensor cGAS which, via STING, besides promoting IFN induction, induces autophagic responses following diverse stimuli including pathogen infection, genotoxic stress, chromosomal instability or aneuploidy, and mitochondrial damage[5–9]. cGAS-STING activation induces "classical" p62/SQSTM1-mediated autophagy as well as "non-canonical" autophagy or CASM (conjugation of ATG8 to single membranes)[10–18]. However, the molecular details of how cGAS-STING signaling triggers autophagy, as well as the downstream mediators involved in this response, are incompletely understood.

The autophagy machinery confines unwanted cellular cargo including damaged organelles, molecular aggregates, and invading pathogens (e.g., viruses) inside well-organized double-membrane vesicles called 'autophagosomes', which prompts cargo degradation

[1]Florida Research and Innovation Center, Cleveland Clinic, Port St. Lucie, FL, USA. [2]Department of Microbiology, The University of Chicago, Chicago, IL, USA. [3]Institute of Molecular Virology, Ulm University Medical Center, Ulm, Germany. [4]The Critical Care Medicine and Pulmonary Branch; National Heart, Lung, and Blood Institute, National Institutes of Health, Bethesda, MD, USA. [5]St. Giles Laboratory of Human Genetics of Infectious Diseases, Rockefeller Branch, The Rockefeller University, New York, NY, USA. [6]Laboratory of Human Genetics of Infectious Diseases, Necker Branch, INSERM U1163, Necker Hospital for Sick Children, Paris, France. [7]Paris Cité University, Imagine Institute, Paris, France. [8]Howard Hughes Medical Institute, New York, NY, USA. [9]German Center for Neurodegenerative Diseases (DZNE), Ulm, Germany. [10]Present address: Eisai GmbH, Frankfurt am Main, Germany. [11]These authors contributed equally: Dhiraj Acharya, Zuberwasim Sayyad. e-mail: gackm@ccf.org

upon fusion with lysosomes[19]. Autophagic flux is triggered by many different viruses (RNA viruses and DNA viruses alike) and, dependent on the specific virus, can positively or negatively impact viral replication and pathogenesis[2,4,20]. In the case of herpes simplex viruses (i.e., HSV-1 and -2), autophagy is important for viral clearance and the control of HSV-induced neuroinflammation and meningitis[4,21–23]. As such, targeting autophagy holds therapeutic promise for a variety of viral and inflammation-associated diseases.

Members of the *tripartite motif* (TRIM) protein family (~80 proteins in humans) belong to the larger RING ubiquitin E3 ligase superfamily[24,25]. In addition to the RING domain, TRIM proteins generally possess one or two B-box modules (of largely unknown function), a coiled-coil domain (for oligomerization), and a C-terminal domain (e.g., a PRY-SPRY domain in ~60% of TRIMs) typically mediating protein/substrate binding[26]. Through catalysis of ubiquitination, ISGylation, and SUMOylation events, TRIM proteins orchestrate a range of cellular processes, including host PRR signaling and antiviral cytokine responses. A subset of TRIM proteins directly engages with viral components, functioning as antiviral restriction factors (e.g., TRIM19/PML, TRIM5α)[26–28]. Recently, several TRIMs, including TRIM23 and TRIM2/3/71, were identified as key regulators of autophagy during viral infection[24,29–31]. How virus infection induces TRIM protein activation and how TRIM proteins orchestrate PRR-mediated autophagy is largely elusive.

HSV-1 is a well-known inducer of classical autophagy that, in turn, limits HSV-1 replication; however, how HSV-1 infection triggers autophagy is still unclear. Here we show that TRIM23 is pivotal for autophagic control of HSV-1 infection and pathology (i.e., encephalitis), and that this activity is independent of type I IFN induction. Our work further indicates that cGAS-STING activation is the major driver of HSV-1-induced classical autophagy where cGAS-STING signaling prompts TBK1 to induce TRIM23 phosphorylation at S39 in its RING domain, promoting TRIM23 activation and ultimately p62-dependent autophagy to suppress HSV-1 replication.

Results

TRIM23 is crucial for autophagic control of HSV-1 infection and pathology

TRIM23 is a crucial regulator of virus-induced autophagy[30]; however, its in vivo relevance in autophagic control of viral infection and pathogenesis is unknown. Autophagy is essential for controlling HSV-1 replication in multiple cell types, including neurons, where it exerts a protective role against HSV-1-induced CNS pathology[22,23,32,33]. We regenerated *Trim23* knockout (*Trim23*$^{-/-}$) mice[34] (Supplementary Fig. 1a and Methods) and tested the physiological role of TRIM23 in autophagy during HSV-1 infection of the central nervous system (CNS). *Trim23*$^{-/-}$ mice exhibited significantly increased mortality as compared to control mice upon intracranial infection with wildtype (WT) HSV-1 (Supplementary Fig. 1b), and this phenotype was even more pronounced when challenged with a Beclin-1-binding-deficient mutant γ34.5 recombinant HSV-1 that is impaired in autophagy antagonism (hereafter called mutHSV-1)[35] (Fig. 1a). mutHSV-1-infected *Trim23*$^{-/-}$ mice showed enhanced viral titers (by ~1.5-log) and elevated viral *ICP-0*, *ICP-8*, *UL36* and *gB* transcripts (by ~20- to 60-fold) in the brain as compared to infected WT control mice (Fig. 1b, c). Immunohistochemical analysis also showed markedly increased HSV-1 antigen expression and viral dissemination in multiple regions of the brain of *Trim23*$^{-/-}$ mice compared with WT control mice (Fig. 1d).

We next compared autophagy in mutHSV-1-infected *Trim23*$^{-/-}$ and WT mice by assessing the protein abundance of endogenous p62, a key autophagy receptor which is degraded in response to autophagic flux[36,37]. mutHSV-1-infected *Trim23*$^{-/-}$ mice showed markedly enhanced p62 protein abundance (indicative of defective autophagy) in the brain compared to infected WT control mice (Fig. 1e, and Supplementary Fig. 1c). Correlated with this phenotype of defective autophagy, robust expression of HSV-1 antigen was detected in the brains of infected *Trim23*$^{-/-}$ mice (in comparison to WT mice), strengthening that TRIM23-mediated autophagy is crucial for restriction of the virus (Supplementary Fig. 1c).

TRIM23 reportedly also regulates cytokine responses (of note, TRIM23's role in cytokine regulation has been studied so far primarily in the context of RNA virus infection[38,39]). We observed similar and a trend of higher transcript expression for *Ifnb1* and *Oas1b* (a representative ISG) in the brains of mutHSV-1-infected *Trim23*$^{-/-}$ mice (as compared to WT mice) at day 2 and 3 post-infection, respectively (Supplementary Fig. 1d), which supports the concept that defective HSV-1 restriction in *Trim23*$^{-/-}$ mice is not due to impaired antiviral cytokine responses.

We next assessed the role of TRIM23 in autophagy regulation in different cell types that are physiologically relevant for HSV-1 infection (i.e., murine neuroblastoma (Neuro2a), human neuroblastoma (SH-SY5Y), and primary human dermal fibroblasts (HDFs)). mutHSV-1 infection triggered robust autophagic degradation of p62 in these cells (Supplementary Fig. 1e), which is consistent with previous reports[40–42]. In line with our data from *Trim23*$^{-/-}$ mice, we observed enhanced mutHSV-1 replication and impaired p62 degradation and LC3B-I-to-II conversion in these cell types upon siRNA-mediated depletion of TRIM23, as compared to cells transfected with non-targeting control siRNA, indicating cell-intrinsic control of HSV-1 infection by TRIM23-mediated autophagy (Fig. 1f–k; and Supplementary Fig. 1f–i). Collectively, these data show that TRIM23 is crucial for autophagic control of HSV-1 infection in various human and mouse cell types, and further, that TRIM23 deficiency exacerbates HSV-1-induced CNS pathology in mice.

TRIM23 mediates HSV-1 restriction via autophagy but not interferon responses

TRIM23 modulates cytokine responses to RNA virus infection, and both cytokine-boosting and -damping roles for TRIM23 have been reported in this context[38,39]. We observed a trend of higher *Ifnb1* and ISG transcript induction in whole brain homogenates of mutHSV-1-infected *Trim23*$^{-/-}$ mice as compared to infected WT control mice, as described above (Supplementary Fig. 1d). Since antiviral gene expression analysis in whole brain might not allow to see clear differences for virus induced cell-intrinsic effects because only a fraction of brain cells is infected, we tested the effect of TRIM23 silencing on cytokine and ISG responses to HSV-1 infection in vitro. We observed a significantly higher transcript expression of *IFNB1*, *TNF*α and ISGs (i.e., *IFIT1, MX1* and *RSAD2*) in *TRIM23*-depleted cells following HSV-1 infection, as compared to infected control cells (Supplementary Fig. 2a, b). These results suggest that TRIM23 negatively regulates cytokine induction during HSV-1 infection, and/or that the enhanced cytokine responses in HSV-1-infected *TRIM23*-deficient cells might be a consequence of the enhanced HSV-1 replication in these cells (see Fig. 1j).

Silencing of TRIM23 enhanced mutHSV-1 replication in mouse embryonic fibroblasts deficient in the IFN-α/β receptor subunit 1 (*Ifnar1*$^{-/-}$ MEFs) to equivalent levels as it did in WT MEFs (Supplementary Fig. 2c), strengthening the proposal that TRIM23 suppresses HSV-1 replication via autophagy but not type I IFN responses. In accord, siRNA-mediated knockdown of TRIM23 increased mutHSV-1 titers in human STAT2-deficient 2fTGH cells (U6A) and WT control cells to comparable levels, and similarly to silencing of ATG5 (autophagy related 5), which is a key regulator of autophagy (Supplementary Fig. 2d, e). Furthermore, TRIM23 efficiently induced autophagy in cells in which IFNAR signaling was ablated using an IFNAR2-blocking antibody (Supplementary Fig. 2f, g), indicating that type I IFN signaling is dispensable for TRIM23's autophagy activity. Together, these results

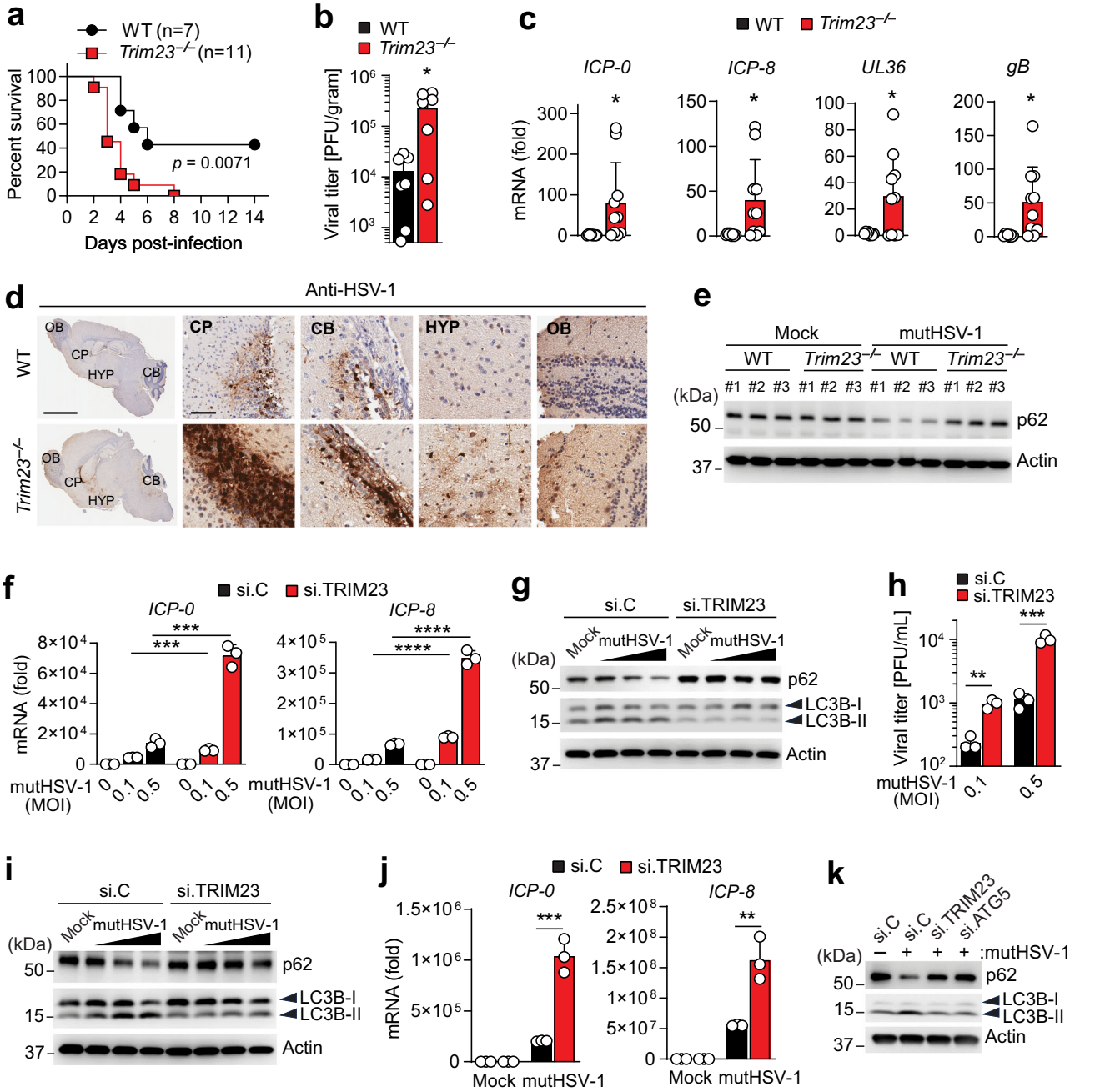

indicate that TRIM23 blocks HSV-1 replication via autophagy but not antiviral IFN responses.

RING phosphorylation at S39 activates TRIM23's E3 ligase activity

TRIM23's RING E3 ligase activity mediates K27-linked auto-poly-ubiquitination, which ultimately promotes p62-dependent autophagy in response to virus infection[30]. However, how TRIM23 is activated by upstream signaling mediators is unknown. As post-translational modifications (PTMs) are well-known to regulate protein functions, we performed large-scale affinity purification of FLAG-tagged TRIM23 from HEK293T cells followed by liquid chromatography coupled with tandem mass spectrometry (LC-MS/MS) to identify PTMs that might regulate TRIM23's activity. This identified phosphorylation at serine 39 (S39) in TRIM23, a conserved residue located in the RING domain (Fig. 2a–c). To monitor TRIM23 phosphorylation at S39 in mammalian cells, we generated a phospho-specific S39 TRIM23 antibody (anti-p-S39-TRIM23) using the 15 amino acid peptide surrounding the phospho-site [$_{32}$GVCEDVFS̲LQGDKVP$_{46}$]. Immunoblot (IB) analysis showed that this antibody reacted strongly with FLAG-tagged TRIM23 WT, but not with a TRIM23 mutant in which S39 was replaced with alanine (S39A) (Fig. 2d). Of note, TRIM23, which –when overexpressed in cells– induces autophagic flux even without stimulation (e.g., virus infection)[30], exhibited a low but detectable level of S39 phosphorylation in uninfected cells, which was markedly enhanced upon mutHSV-1 infection (Fig. 2e). Moreover, the enhanced S39 phosphorylation of FLAG-TRIM23 in mutHSV-1-infected cells correlated with strongly increased ubiquitination levels of TRIM23 (Fig. 2e). Importantly, both WT HSV-1 and mutHSV-1 induced robust S39 phosphorylation of endogenous TRIM23 (Fig. 2f, g; and Supplementary Fig. 3a). Furthermore, endogenous TRIM23 phosphorylation at S39 could be detected as early as 8 h post mutHSV-1 infection, and this phosphorylation increased over the course of infection (Fig. 2h, i). Consistent with our data in human cells, we observed S39 phosphorylation of TRIM23 in

Fig. 1 | TRIM23 regulates HSV-1 pathogenesis and autophagy in vivo. **a**–**e** *Trim23*$^{-/-}$ mice and wild type (WT) littermate controls of both sexes (8-week-old, sex-matched across treatments) were infected via intracerebral (I.C.) inoculation with 5×10^5 PFU of mutHSV-1. **a** Kaplan–Meier survival curves of mutHSV-1-infected *Trim23*$^{-/-}$ and WT mice. **b** Viral titers in whole brain homogenates of *Trim23*$^{-/-}$ and WT mice, determined by plaque assay at day 3 post-infection. **c** HSV-1 *ICP-0*, *ICP-8*, *UL36* and *gB* transcripts in whole brain homogenates, determined by RT-qPCR at day 3 post-infection. **d** HSV-1 antigen expression in the indicated areas of mid-sagittal brain sections of mutHSV-1-infected *Trim23*$^{-/-}$ and WT mice, determined at day 3 post-infection by immunohistochemistry. Scale bar, 3 mm (whole brain) or 50 μm (magnified areas). CP, caudate putamen; CB, cerebellum; HYP, hypothalamus; OB, olfactory bulb. **e** Endogenous p62 protein abundance in the whole brain lysates of mock-treated or mutHSV-1-infected *Trim23*$^{-/-}$ and WT mice, determined at day 3 post-infection by immunoblot (IB). #1–#3 represent individual mice. **f** Viral *ICP-0* and *ICP-8* transcript expression in Neuro2a (mouse neuroblast) cells that were transfected for 30 h with the indicated siRNAs and then infected for 36 h with mutHSV-1 at the indicated MOIs, determined by RT-qPCR. **g** Endogenous p62 protein abundance and LC3B-I-to-II conversion in the whole cell lysates (WCLs) of Neuro2a cells that were transfected for 30 h with the indicated siRNAs and then either mock-treated or infected with mutHSV-1 (MOI 1, 5, and 10) for 24 h, determined by IB. **h** Viral titers in SH-SY5Y (human neuroblastoma) cells that were transfected for 30 h with the indicated siRNAs and then infected for 24 h with mutHSV-1 at the indicated MOIs, determined by plaque assay. **i** Endogenous p62 protein abundance and LC3B-I-to-II conversion in the WCLs of SH-SY5Y cells that were transfected for 30 h with the indicated siRNAs and then either mock-treated or infected with mutHSV-1 (MOI 0.2, 1 and 2) for 20 h, determined by IB. **j** Viral *ICP-0* and *ICP-8* transcript expression in primary human dermal fibroblasts (HDFs) that were transfected for 30 h with the indicated siRNAs and then either mock-treated or infected with mutHSV-1 (MOI 0.02) for 24 h, determined by RT-qPCR. **k** Endogenous p62 protein abundance and LC3B-I-to-II conversion in the WCLs of HDFs that were transfected for 30 h with the indicated siRNAs and then either mock-treated (−) or infected with mutHSV-1 (MOI 10) for 16 h, determined by IB. All data (**a** to **k**) are representative of at least two independent experiments ($n = 7$ mice for WT and $n = 11$ mice for *Trim23*$^{-/-}$ (**a**); mean ± SD of $n = 7$ mice per condition (**b**); mean ± SD $n = 8$ mice for WT and $n = 10$ mice for *Trim23*$^{-/-}$ (**c**); mean ± SD of $n = 3$ biological replicates (**f**, **h** and **j**)). $^*p < 0.05$, $^{**}p < 0.01$, $^{***}p < 0.001$, $^{****}p < 0.0001$ (Mantel–Cox log rank test (**a**), two-tailed Student's t test with Welch's correction (**b**, **c**), or two-tailed Student's t test (**f**, **h** and **j**). Source data are provided as a Source Data file.

mouse cells infected with mutHSV-1 but not in uninfected cells (Supplementary Fig. 3b, c).

We next looked at the crystal structure of the TRIM23 RING dimer in complex with an ubiquitin (Ub)-loaded E2 enzyme[43]. This showed that the S39 loop is stabilized in part by a bifurcated hydrogen bond from the S39 sidechain, suggesting that phosphorylation of S39 may alter the loop conformation and thereby perhaps Ub and/or E2 binding, which is expected to affect TRIM23's E3 ligase activity (Fig. 2j). To test this, we compared the K27-linked auto-ubiquitination of WT TRIM23 with that of the non-phosphorylatable S39A mutant. We also included in this experiment two phosphomimetic TRIM23 mutants which harbor aspartic or glutamic acid in place of serine 39 (S39D or S39E). The S39A mutant exhibited a near-complete loss of K27-linked ubiquitination, whereas the S39D and S39E mutants showed comparable ubiquitination levels with WT TRIM23 (Fig. 2k). Collectively, these data indicate that TRIM23 RING phosphorylation at S39 is important for efficient E3 ubiquitin ligase activity.

S39 phosphorylation promotes TRIM23 GTPase activity and antiviral autophagy

RING-mediated auto-ubiquitination of the ARF domain facilitates TRIM23's ARF GTPase activity, which is required for TRIM23-induced antiviral autophagy[30]. Therefore, we next asked whether S39 phosphorylation affects the GTPase activity of TRIM23. Notably, the S39A 'phospho-null' mutant had a strongly impaired GTPase activity as compared to WT TRIM23, whereas the phosphomimetic S39D and S39E mutants exhibited efficient GTPase activity (Fig. 3a). TRIM23 ΔARF, which is defective in GTPase activity, and Rab5α (a small GTPase) served as controls. Next, we used HeLa cells that stably express green fluorescent protein (GFP)-fused LC3B to examine the ability of TRIM23 WT and mutants to induce GFP-LC3B puncta formation[30,37]. In line with their GTPase activities, TRIM23 WT and the S39D and S39E mutants robustly induced GFP-LC3B puncta (Fig. 3b, c). In contrast, the TRIM23 S39A mutant only marginally elicited GFP-LC3B puncta formation (Fig. 3b, c). Similarly, WT TRIM23 and the two phosphomimetic mutants S39D and S39E, but not the S39A mutant, effectively promoted LC3B-I-to-II conversion (Fig. 3d).

A key function of the C-terminal GTPase activity is to translocate TRIM23 to autophagosomes where it colocalizes with the autophagy receptor p62[30]. Whereas the S39A mutant failed to colocalize with endogenous p62, WT TRIM23 and the S39D and S39E mutants extensively colocalized with p62 (Fig. 3e, f). Interestingly, ectopically expressed WT TRIM23 and the S39D and S39E mutants formed defined puncta in the cytoplasm, while the S39A mutant did not (Fig. 3e). We next tested the relevance of S39 phosphorylation for TRIM23's ability to inhibit HSV-1 replication. Ectopically expressed WT TRIM23 and the S39D and S39E mutants, but not the S39A mutant, effectively restricted mutHSV-1 infection (Fig. 3g, h). Altogether, these findings show that RING S39 phosphorylation is required for TRIM23's ability to elicit autophagy and to suppress HSV-1 replication.

TBK1 phosphorylates TRIM23 at S39 to induce autophagy

To identify the kinase(s) responsible for TRIM23 S39 phosphorylation, we performed bioinformatics prediction analysis (see "Methods") of potential candidate kinases for the $_{32}$GVCEDVFSLQGDKVP$_{46}$ motif in TRIM23. This identified nine candidate kinases (STK38, ATR, AMPKα2, MAP3K5, LRRK1, IKKε, TBK1, RIPK2, and ROCK1). In addition, we selected PINK1 and IKKβ, which are known to induce autophagy[44–46]. We subjected these 11 candidate kinases to a targeted RNAi screen to test the effect of kinase knockdown on S39 phosphorylation of TRIM23-FLAG (Fig. 4a; Supplementary Fig. 4a). This analysis showed that silencing of endogenous TBK1 markedly reduced S39 phosphorylation of TRIM23, while the other kinases tested had either no or only a marginal effect on TRIM23 S39 phosphorylation (Fig. 4a; Supplementary Fig. 4b). Ectopically expressed TBK1, but not IKKβ (a related kinase), enhanced TRIM23 S39 phosphorylation in a dose-dependent manner (Fig. 4b). Notably, WT TBK1, but not the kinase-dead mutants K38A and S172A, promoted the phosphorylation of TRIM23-FLAG at S39 (Fig. 4c), further strengthening that the potentiating effect on TRIM23 phosphorylation is not an indirect effect of TBK1. Recombinant TBK1 robustly induced S39 phosphorylation of purified GST-TRIM23 in an in vitro kinase assay (Fig. 4d), which demonstrates that TRIM23 is a direct substrate of TBK1.

As S39 phosphorylation mediates critical activation steps in TRIM23 (i.e., its K27-linked auto-ubiquitination and GTPase activity), we next asked if TBK1 promotes these molecular events. Ectopic expression of TBK1 enhanced TRIM23-FLAG polyubiquitination in a dose-dependent manner, which correlated with enhanced S39 phosphorylation (Supplementary Fig. 4c). Conversely, the phosphorylation (at S39) and polyubiquitination of TRIM23-FLAG were reduced in a dose-dependent manner upon chemical inhibition of endogenous TBK1 by BX795 (Fig. 4e). Consistent with this, mutHSV-1-induced S39 phosphorylation of endogenous TRIM23 was ablated upon BX795 treatment (Fig. 4f, g).

Proximity ligation assay (PLA) showed a close spatial proximity of endogenous p-S39-TRIM23 and p-S172-TBK1 in cells infected with WT HSV-1 or mutHSV-1 but not in uninfected cells (Fig. 4h). To corroborate

https://doi.org/10.1038/s41467-025-59338-5

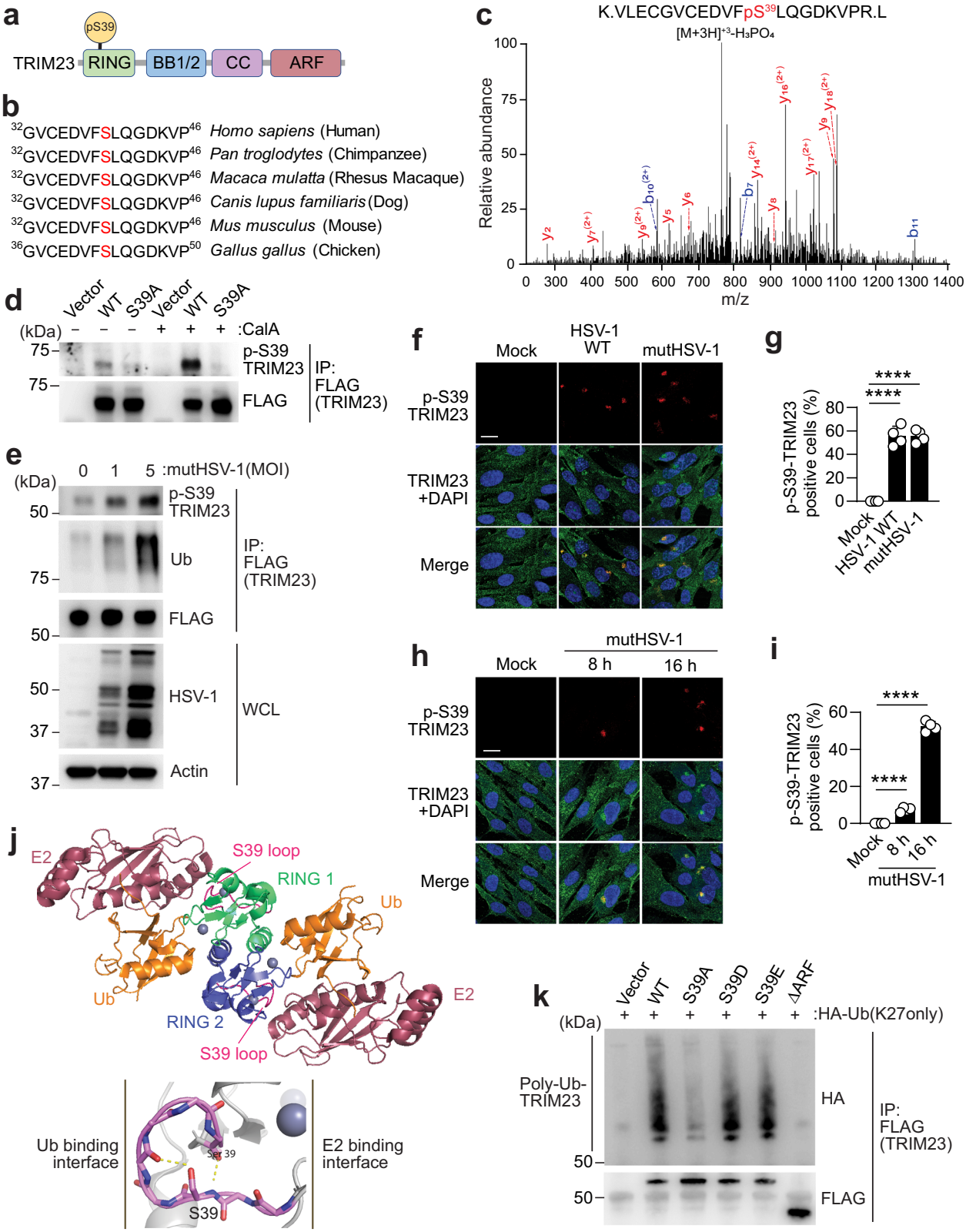

that TBK1 is a primary kinase mediating TRIM23 phosphorylation to induce autophagy, we generated clonal *TBK1* knockout (KO) cell lines (i.e., HEK293T and A549) by CRISPR-Cas9 gene editing (Supplementary Fig. 4d, e). We observed a complete loss of TRIM23 S39 phosphorylation in *TBK1* KO cells (Fig. 4i). Importantly, reconstitution of *TBK1* KO cells with WT TBK1 restored the phosphorylation of WT TRIM23, but not of the S39A mutant, which served as a control (Fig. 4j). Furthermore, ectopic expression of WT TRIM23 robustly induced GFP-LC3B puncta formation in WT control cells, but not in *TBK1* KO cells (Fig. 4k, l). In contrast, the TRIM23 S39A 'phospho-null' mutant did not induce GFP-LC3B puncta formation in either WT or *TBK1* KO cells, as expected. Notably, the TRIM23 S39E phosphomimetic mutant, which does not rely on TBK1 for its activation, triggered GFP-LC3B puncta formation in WT control and *TBK1* KO cells to similar levels (Fig. 4k, l).

Fig. 2 | TRIM23 is phosphorylated at Ser-39. a Schematic representation of the domain organization of TRIM23 with the phospho-S39 (pS39) residue illustrated. RING, Really Interesting New Gene domain; BB1/2, B-Box 1 and 2; CC, coiled-coil domain; ARF, ADP-ribosylation factor domain. **b** Amino acid sequence of the region containing the S39 residue in TRIM23 from the indicated species. Numbers indicate amino acid positions. **c** Tandem mass spectra of the tryptic peptide K.VLECGVCEDVFpS_{39}LQGDKVPR.L of TRIM23-FLAG affinity-purified from transiently transfected HEK293T cells that identified phosphorylation at S39. **d** Phosphorylation of TRIM23-FLAG WT and S39A mutant in transiently transfected HEK293T cells that were either mock-treated (−) or treated with calyculin A (Cal A, a phosphatase inhibitor), determined at 48 h post-transfection by immunoprecipitation (IP) with anti-FLAG and IB with anti-p-S39-TRIM23 antibody. **e** S39 phosphorylation and poly-ubiquitination of FLAG-TRIM23 stably expressed in HDFs that were infected with mutHSV-1 as indicated, determined at 8 h post-infection by IP with anti-FLAG and IB with anti-p-S39-TRIM23 or anti-ubiquitin (Ub). **f** S39 phosphorylation of endogenous TRIM23 in HDFs that were either mock-treated or infected with WT HSV-1 or mutHSV-1 (MOI 5 for both) for 16 h, determined by immunostaining with the indicated antibodies and confocal microscopy analysis. DAPI, nuclei (blue). Scale bar, 20 μm. **g** Quantification of p-S39-TRIM23-positive cells for the data shown in (**f**). **h** Time course analysis of endogenous TRIM23 S39 phosphorylation in HDFs that were either mock-treated or infected with mutHSV-1 (MOI 5) for the indicated times, determined as in (**f**). DAPI, nuclei (blue). Scale bar, 20 μm. **i** Quantification of p-S39-TRIM23-positive cells for the data shown in (**h**). **j** Upper: Ribbon representation of the crystal structure of the TRIM23-RING dimer (green/blue) in complex with Ub-loaded E2 (orange/red)[43]. The loops containing S39 are highlighted in pink. Lower: Close-up view of the RING S39 loop, stabilized in part by a bifurcated hydrogen bond (yellow), and its proximity to the Ub or E2 binding interface. **k** K27-linked auto-polyubiquitination of FLAG-tagged TRIM23 WT or mutants in transiently transfected HEK293T cells that co-expressed an HA-tagged ubiquitin mutant (HA-Ub-K27only), determined at 48 h post-transfection by IP with anti-FLAG and IB with anti-HA. Data in (**c**) are from one unbiased MS analysis, data in (**d**–**i** and **k**) are representative of at least two independent experiments (mean ± SD of $n = 4$ biological replicates (**g**, **i**). $^{****}p < 0.0001$ (two-tailed Student's t test (**g**, **i**). Source data are provided as a Source Data file.

Collectively, these results support the conclusion that TRIM23 S39 phosphorylation by TBK1 promotes autophagy.

cGAS prompts TBK1-mediated TRIM23 S39 phosphorylation for autophagy induction

TBK1 is activated downstream of multiple PRRs in response to virus infection, leading to IRF3/7-mediated type I/III IFN responses[47]. However, the molecular events by which TBK1 is activated to elicit autophagy during virus infection are unknown. We hypothesized that specific PRR(s) trigger TBK1 activation and thereby TRIM23 S39 phosphorylation, ultimately inducing autophagic responses to HSV-1 infection. As is true for most viral infections, several PRRs are implicated in HSV-1 sensing (of note, these sensors have been extensively studied mainly for their roles in IFN induction)[48–50]. Among these are the intracellular DNA sensor cGAS that recognizes HSV-1 dsDNA[51], the cytoplasmic receptors RIG-I and MDA5 which detect cellular or virus-derived RNA species (e.g., the host small noncoding RNA, *RNA5SP141*, in the case of RIG-I[52,53]), and TLR3 and TLR9 that recognize, respectively, endosomally residing dsRNA and dsDNA[54,55]. Silencing of endogenous cGAS, but not of the other sensors, markedly reduced p62 degradation in mutHSV-1-infected primary HDFs as compared to transfection of non-targeting control siRNA (Fig. 5a; and Supplementary Fig. 5a, b). Of note, as silencing of these innate immune sensor or signaling proteins may affect HSV-1 infection or replication, we used a high MOI of HSV-1 in this assay to ensure comparable infection in the different knockdown samples. Notably, the effect of cGAS knockdown on p62 protein abundance was similar to that of depletion of TRIM23, TBK1 or ATG5, which served as controls in this experiment (Fig. 5a; and Supplementary Fig. 5b). In line with these results, depletion of cGAS impaired mutHSV-1-induced LC3B-I-to-II conversion to similar levels as TRIM23 or ATG5 knockdown (Supplementary Fig. 5c). We also observed that mutHSV-1-induced LC3B-I-to-II conversion and p62 degradation is ablated upon STING silencing (Supplementary Fig. 5d), suggesting that primarily cGAS-STING signaling mediates HSV-1-induced autophagy in dermal fibroblasts. Conversely, ectopic expression of FLAG-cGAS and FLAG-STING robustly triggered endogenous p62 degradation and LC3B-I-to-II conversion, as previously reported[11,56] (Supplementary Fig. 5e). In comparison, expression of FLAG-tagged RIG-I, MDA5, MAVS or IRF3-5D (a constitutively active form of IRF3 in eliciting IFN induction) only minimally triggered autophagy flux (Supplementary Fig. 5e). Notably, these sensor and adaptor proteins as well as IRF3-5D effectively potentiated the expression of IFIT1, a representative ISG that was included as a control to confirm that the expressed innate immune proteins are signaling competent under these conditions (Supplementary Fig. 5e). Taken together, these results suggest that cGAS-STING signaling is a primary driver of p62-dependent autophagy during HSV-1 infection.

In support of this concept, stimulation of primary HDFs with the dsDNA ligands poly(dG:dC)-LyoVec, poly(dA:dT)-LyoVec, and interferon-stimulatory DNA (ISD)-LyoVec effectively elicited GFP-LC3B puncta formation and LC3B-I-to-II conversion (Supplementary Fig. 5f–h). Stimulation of cells with poly(I:C)-LyoVec (sensed by MDA5 and RIG-I) also triggered GFP-LC3B puncta formation and LC3B-I-to-II conversion, although less efficiently than dsDNA stimulation under these conditions (Supplementary Fig. 5f–h) (of note, differential autophagy-inducing potencies of dsDNA vs. dsRNA agonists have been reported previously[11]). Consistent with this, stimulation of HDFs with poly(dG:dC)-LyoVec or ISD-LyoVec, but not with poly(I:C)-LyoVec, potently elicited S39 phosphorylation of endogenous TRIM23 (Fig. 5b, c). We also observed enhanced TRIM23 phosphorylation and ubiquitination upon ectopic expression of cGAS and STING as compared to vector co-expression (Fig. 5d). Interestingly, overexpression of FLAG-RIG-I did not induce these TRIM23 activation steps (Fig. 5d), hinting at unique signaling events and/or mediators downstream of cGAS that facilitate TRIM23 activation via TBK1. Consistent with its potentiating effect on TRIM23 S39 phosphorylation, activation of cGAS-STING signaling by poly(dG:dC)-LyoVec increased TRIM23 ubiquitination (Fig. 5e). Ectopically expressed cGAS and STING also promoted TRIM23's GTPase activity (Supplementary Fig. 5i), strengthening the proposal that the cGAS-STING pathway leads to full TRIM23 activation.

We next assessed the role of TRIM23 and TBK1 in mediating cGAS-STING-induced autophagy. siRNA-mediated knockdown of endogenous TRIM23, TBK1, or ATG5 (control) impaired LC3B-I-to-II conversion induced by co-expression of cGAS and STING (Supplementary Fig. 5j, k). Of note, no such effect was observed upon depletion of IRF3, suggesting that the cGAS-TBK1-TRIM23 axis mediates autophagy independently of IRF3 (Supplementary Fig. 5j, k). In accord, TRIM23 or TBK1 depletion, but not IRF3 silencing, markedly reduced the formation of GFP-LC3B puncta elicited by poly(dG:dC)-LyoVec stimulation (as compared to si.C transfection) (Fig. 5f, g). Notably, whereas the diminishing effect of TRIM23 depletion on GFP-LC3B puncta formation was comparable to that observed for ATG5 knockdown, silencing of TBK1 reduced LC3B puncta slightly less efficiently, suggesting TBK1-dependent (via TRIM23) and TBK1-independent autophagy activation downstream of cGAS stimulation[11–13]. Consistent with our other data revealing TRIM23 as a key mediator of cGAS-induced autophagy, LC3B-I-to-II conversion and p62 phosphorylation (at S403) induced by poly(dG:dC)-LyoVec stimulation were impaired upon TRIM23 silencing (Fig. 5h, i). TRIM23 depletion also diminished p62 degradation and its phosphorylation (at S403) following ectopic expression of cGAS and STING (Fig. 5j; and Supplementary Fig. 5l). We also observed that cGAMP-induced LC3B-I-to-II conversion and p62 degradation is ablated upon TRIM23 silencing (Supplementary Fig. 5m). Finally, we tested

https://doi.org/10.1038/s41467-025-59338-5

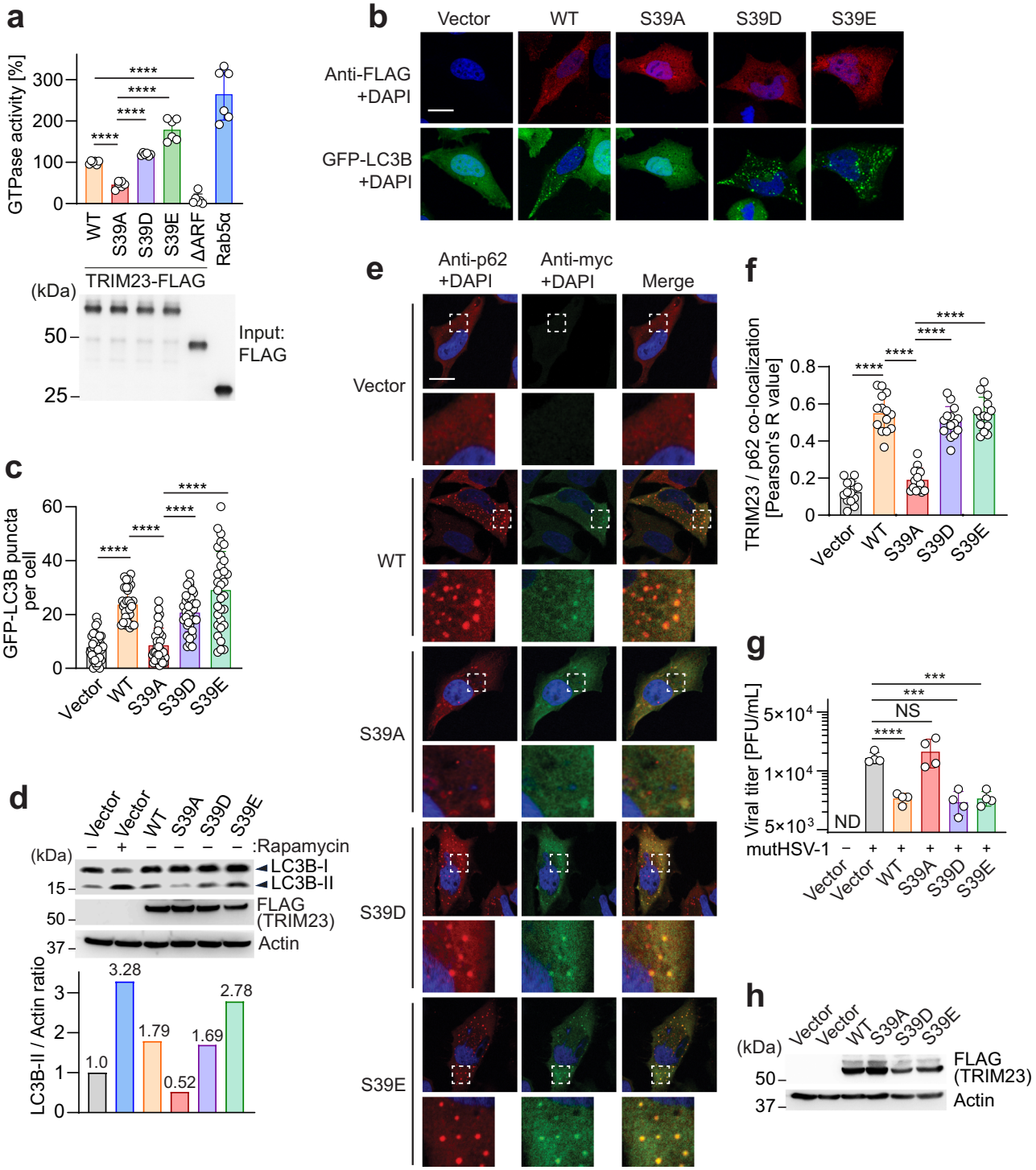

the colocalization of p-S39-TRIM23 with p-S172-TBK1 following poly(dG:dC)-LyoVec stimulation by PLA. This showed a close spatial proximity of p-S39-TRIM23 and p-S172-TBK1 in poly(dG:dC)-LyoVec-stimulated cells, but not in mock-treated cells (Fig. 5k, l). Collectively, these results establish that cGAS stimulation elicits TBK1-mediated TRIM23 phosphorylation and activation and thereby autophagy.

TBK1-TRIM23 feed-forward activation loop that is dictated by distinct subcellular localizations

TRIM23 activates p62-dependent autophagy in response to HSV-1 infection[30]. Our previous study showed that the activation of TRIM23's GTPase function via auto-ubiquitination facilitates TBK1 oligomerization and thereby *trans*-auto-phosphorylation, promoting p62 phosphorylation by TBK1[30]. The data presented herein indicate that TBK1 directly phosphorylates TRIM23, which licenses TRIM23 activation, suggesting an intricate cross-regulation between TRIM23 and TBK1 as part of a feed-forward activation circuit. To investigate this regulatory loop further, we first asked whether TRIM23-TBK1 complex formation requires TRIM23 auto-ubiquitination-dependent activation. Interestingly, the TRIM23 C34A mutant, which is E3 ligase-defective (and hence has ablated GTPase function)[30], bound to TBK1 as efficiently as WT TRIM23 (Supplementary Fig. 6a). By contrast, TRIM23 ΔARF was unable to interact with TBK1, as previously shown[30]. Moreover, TRIM23 C34A and the GTPase-dead mutant

Fig. 3 | Phosphorylation at S39 regulates TRIM23-mediated autophagy and antiviral activity. a Top: GTPase enzymatic activity of FLAG-tagged TRIM23 WT and indicated mutants, or FLAG-tagged Rab5α (positive control), that were affinity purified by IP using anti-FLAG from transiently transfected HEK293T cells, determined by GTPase Glo assay. Values for WT TRIM23 were set to 100%. Bottom: Expression of the indicated proteins determined by IB. **b** GFP-LC3B puncta formation in HeLa cells stably expressing GFP-LC3B (green) that were transfected with either empty vector or the indicated FLAG-tagged TRIM23 constructs (red), determined at 48 h post-transfection by immunostaining with anti-FLAG followed by confocal microscopy analysis. DAPI, nuclei (blue). Scale bar, 20 μm. **c** Quantification of the number of GFP-LC3B puncta for the data shown in (**b**). **d** Top: Endogenous LC3B-I-to-II conversion in HEK293T cells that were transiently transfected with either empty vector or the indicated TRIM23-FLAG constructs, determined at 48 h post-transfection by IB with the indicated antibodies. Stimulation with rapamycin (3 μM for 4 h) served as a positive control. Bottom: Densitometric analysis of the LC3B-II signal intensities, normalized to the respective actin protein abundances, for the data shown on top. Values for the empty vector control (without rapamycin) were set to 1. **e** Co-localization of transiently expressed myc-tagged TRIM23 (green) with endogenous p62 (red) in HeLa cells, determined at 48 h post-transfection by immunostaining with anti-myc and anti-p62 followed by confocal microscopy analysis. DAPI, nuclei (blue). Scale bar, 20 μm. **f** Quantification of p62-TRIM23 colocalization for the data shown in (**e**), determined by Pearson's correlation coefficient. **g** Viral titers in the supernatant of HEK293T cells that were transfected for 24 h with either empty vector or FLAG-tagged TRIM23 WT or mutants and then either mock-treated (−) or infected with mutHSV-1 (MOI 1) for 24 h, determined by plaque assay. **h** Representative expression of TRIM23-FLAG WT and mutant proteins for the experiment in (**g**), determined in the WCLs at 24 h post-transfection by IB with anti-FLAG and anti-actin (loading control). All data (**a**–**h**) are representative of at least two independent experiments (mean ± SD of $n = 6$ (**a**), $n = 4$ (**g**) biological replicates; mean ± SEM of $n = 37, 30, 32, 34, 32$ cells respectively for vector, WT, S39A, S39D, and S39E (**c**); $n = 14$ cells (**f**). $^{***}p < 0.001$; $^{****}p < 0.0001$ (two-tailed Student's t test with Welch's correction (**a**, **c**, **f**), or two-tailed Student's t test (**g**). NS not significant. ND not detected. Source data are provided as a Source Data file.

K458I were effectively phosphorylated at S39 by TBK1 (Supplementary Fig. 6b), while TRIM23 ΔARF (TBK1-binding-deficient) and TRIM23 ΔRING (lacking S39) were not, suggesting that TBK1 acts as upstream kinase for TRIM23 leading to its activation.

We posited that TRIM23 activation by TBK1-mediated phosphorylation and TRIM23's activity to facilitate p62 activation by TBK1 occur at distinct subcellular locations in a temporal fashion. In support of this concept, we observed a close spatial proximity of endogenous p-S39-TRIM23 with the Golgi marker GM130 at early times upon cGAMP stimulation (Supplementary Fig. 6c, d). At later times, however, p-S39-TRIM23 showed a prominent spatial proximity with ATG16, indicating localization to autophagosomes (Supplementary Fig. 6c, d). These results, together with our previous data[30], suggest an intricate 'feed-forward' activation loop that regulates TBK1-TRIM23-induced autophagy. Specifically, following cGAS-STING activation TRIM23 is initially phosphorylated at S39 by TBK1 at the Golgi apparatus; this phosphorylation event then triggers TRIM23 auto-ubiquitination of the ARF domain promoting GTP-GDP cycling. Subsequently, GTPase activity promotes higher-order assembly of bound TBK1 and trafficking of the TRIM23-TBK1 complex to autophagosomes, ultimately leading to p62 phosphorylation by TBK1.

TRIM23 forms a complex with STING and TBK1 in HSV-1-infected or dsDNA-stimulated cells, leading to TRIM23 phosphorylation

We next examined the spatial and temporal aspects of STING, TRIM23 and TBK1 complex formation after HSV-1 infection or poly(dG:dC) transfection. Endogenous STING extensively co-localized with p-S172-TBK1 after mutHSV-1 infection or poly(dG:dC)-LyoVec stimulation but not in mock-treated cells, as expected (Fig. 6a, b). p-S39-TRIM23 co-localized with p-S172-TBK1 and STING in defined cytoplasmic puncta in mutHSV-1-infected, but not mock-treated, cells (Fig. 6a, b). Similarly, stimulation of cells with poly(dG:dC)-LyoVec also induced co-localization of endogenous p-S39-TRIM23 with STING and p-S172-TBK1, suggesting the formation of a STING-TRIM23-TBK1 ternary complex (Fig. 6a, b). We next performed Co-IP assay to examine the binding of V5-tagged TRIM23 to FLAG-tagged STING. In this experiment, we also included several mutants of STING in which specific domains are deleted or key functional residues mutated[11,18]. These included the STING mutants in which, respectively, the cyclic dinucleotide-binding domain or C-terminal tail is deleted (ΔCBD or ΔCTT), or in which S366, which is important for downstream signaling[57], is mutated (S366A) (Fig. 6c). Co-IP assay showed that TRIM23-V5 efficiently bound FLAG-tagged WT STING and the ΔCTT and S366A mutants, but not the ΔCBD mutant (Fig. 6d). Altogether, these data indicate that upon HSV-1 infection or cGAS-STING activation TRIM23 interacts with the CBD domain of STING and is phosphorylated by co-recruited TBK1, thus promoting TRIM23 activation and hence induction of autophagy.

HSE-associated *TBK1* germline mutation impairs TRIM23 activation and HSV-1-induced autophagy

Germline mutations in the *TBK1* gene that underlie herpes simplex encephalitis (HSE) have been characterized in humans[58]. Among these mutations, the heterozygous TBK1 G159A (c.476 G > G/C) mutation is associated with *TBK1* deficiency through negative dominance of this kinase-defective TBK1 mutant (Supplementary Fig. 7a), resulting in impaired cell-intrinsic control of HSV-1 infection[58,59]. We posited that TBK1 G159A has an impaired ability to phosphorylate and activate TRIM23, thereby leading to defective cellular autophagic responses to HSV-1. Patient fibroblasts carrying the G159A mutation showed impaired endogenous TBK1 phosphorylation (at S172) and ablated LC3B-I-to-II conversion and p62 phosphorylation (at S403) upon HSV-1 infection, indicative of defective autophagy (Fig. 7a; and Supplementary Fig. 7b), which is in line with previous findings[59]. Using *TBK1* KO HEK293T cells reconstituted with either TBK1 WT or G159A, we found that WT TBK1 robustly induced TRIM23 S39 phosphorylation, whereas the G159A mutant failed to phosphorylate TRIM23 (Fig. 7b). The TBK1 K38A and S172A mutants, which are also catalytically inactive and thus served as controls, also failed to mediate TRIM23 S39 phosphorylation (Fig. 7b; and Supplementary Fig. 7a). Moreover, WT TBK1, but not the G159A, K38A and S172A mutants, markedly enhanced TRIM23 auto-ubiquitination (Fig. 7b), which is consistent with our data that RING S39 phosphorylation stimulates TRIM23 K27-linked auto-ubiquitination. In accord, ectopic expression of WT TBK1, but not of the G159A, K38A or S172A mutant, in *TBK1* KO HEK293T cells triggered LC3B-I-to-II conversion, p62 degradation and p62 S403 phosphorylation (Fig. 7c). Importantly, TBK1 G159A (as well as K38A and S172A mutants) interacted with TRIM23 as efficiently as WT TBK1 (Supplementary Fig. 7c), strengthening the notion that the failure of TBK1 G159A to phosphorylate TRIM23 is due to the abolished kinase activity, but not TRIM23-binding ability, of this mutant.

Next, we asked whether the failure of the TBK1 G159A mutant to phosphorylate TRIM23 is responsible for the impaired autophagy response in the patient fibroblasts. Exogenous WT TRIM23, which relies on S39 phosphorylation by TBK1 for its activation, robustly triggered GFP-LC3B puncta formation in healthy control cells, but not in the mutant TBK1 patient cells (Fig. 7d, e). By contrast, TRIM23 S39A minimally induced GFP-LC3B puncta in control and patient cells. Notably, TRIM23 S39E, which is a constitutively active mutant and does not rely on TBK1-mediated phosphorylation for its activation, effectively promoted GFP-LC3B puncta formation in both control and mutant TBK1 fibroblasts (Fig. 7d, e). In accord, immunofluorescence analysis showed that TRIM23 extensively colocalized with p62 in

https://doi.org/10.1038/s41467-025-59338-5

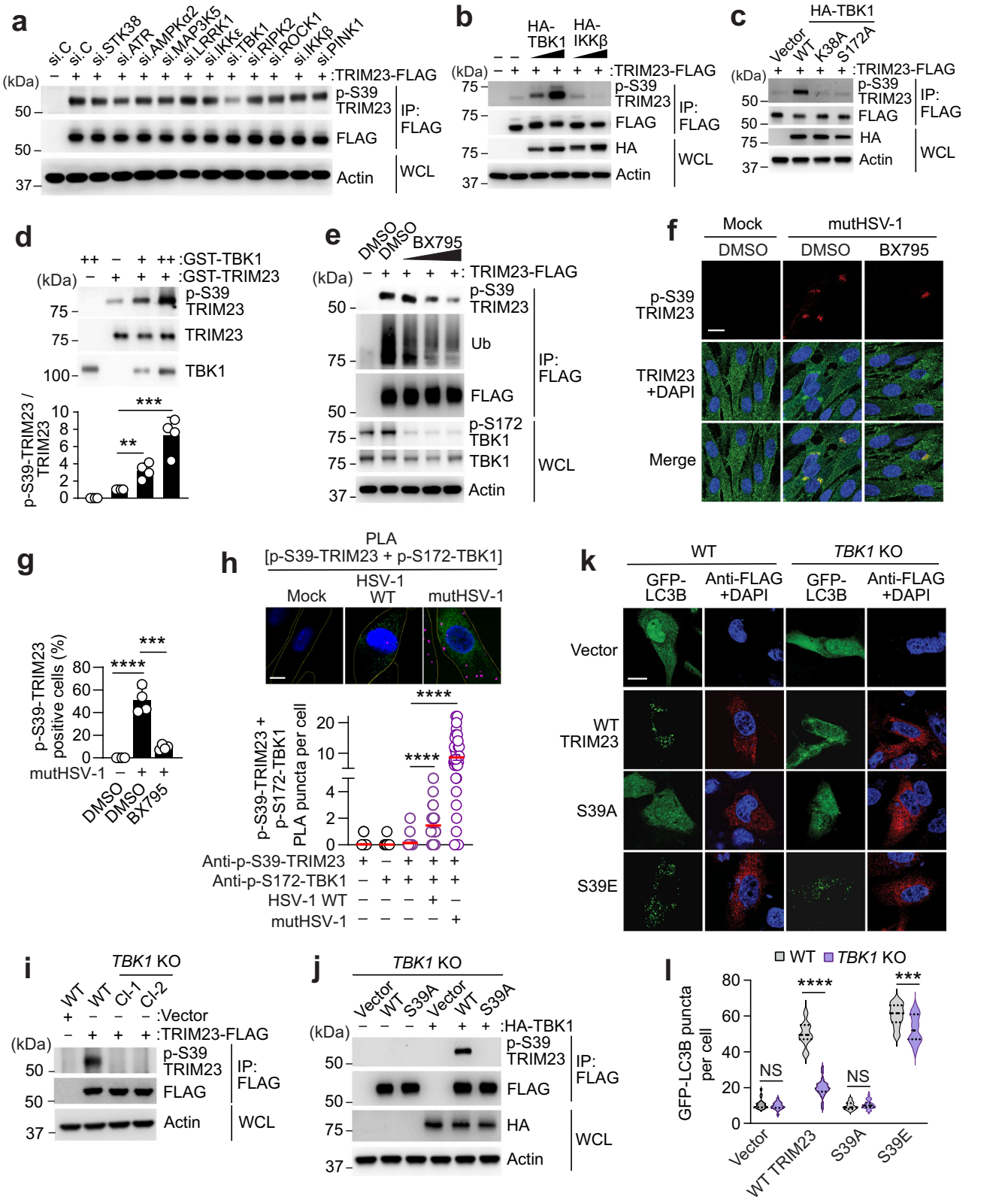

healthy control fibroblasts following mutHSV-1 infection or poly(dG:dC)-LyoVec stimulation (Fig. 7f, g). In contrast, no or only marginal TRIM23-p62 colocalization was observed in infected or stimulated mutant TBK1 fibroblasts (Fig. 7f, g). Taken together, these data suggest that the impaired autophagy in the HSE patient fibroblasts carrying the heterozygous, dominant-negative TBK1 G159A mutation is due to defective phosphorylation-dependent TRIM23 activation.

Discussion

TRIM E3 ligases regulate cellular host defenses by modulating antiviral cytokine production and inflammatory responses[26,60]. Several TRIM family members (such as TRIM23, TRIM5α, TRIM3) also coordinate autophagic responses during virus infection[25,29,31,61]; however, the underlying mechanisms and in vivo relevance of TRIM-mediated autophagy are still largely unknown. Here, we show that mice deficient

Fig. 4 | TBK1 phosphorylates TRIM23 at S39. a S39 phosphorylation of TRIM23-FLAG in HEK293T cells that were co-transfected with the indicated siRNAs, determined at 48 h post-transfection by IP with anti-FLAG and IB with anti-p-S39-TRIM23. **b** S39 phosphorylation of TRIM23-FLAG in HEK293T cells that co-expressed either empty vector (−) or increasing amounts of HA-TBK1 or HA-IKKβ, determined at 48 h post-transfection by IP with anti-FLAG and IB with anti-p-S39-TRIM23. **c** S39 phosphorylation of TRIM23-FLAG in HEK293T cells that co-expressed the indicated HA-tagged TBK1 constructs, determined at 48 h post-transfection by IP with anti-FLAG and IB with anti-p-S39-TRIM23. **d** Top: In vitro kinase assay assessing S39 phosphorylation of purified GST-TRIM23 upon co-incubation with purified GST-TBK1, determined by IB with anti-p-S39-TRIM23, anti-TRIM23 and anti-TBK1. Bottom: Densitometric analysis of the p-S39-TRIM23 signal intensities, normalized to the respective TRIM23 protein abundances, for the data shown on top. **e** S39 phosphorylation and ubiquitination of TRIM23-FLAG in transiently transfected HEK293T cells that were treated with either DMSO or increasing doses of BX795 (0.5, 1 and 2 μM) for 4 h, determined at 48 h post-transfection by IP with anti-FLAG and IB with the indicated antibodies. **f** Endogenous TRIM23 S39 phosphorylation in HDFs that were either mock-treated or infected with mutHSV-1 (MOI 5) for 12 h and then treated for 4 h with either DMSO or BX795 (5 μM), determined by immunostaining with the indicated antibodies and confocal microscopy analysis. DAPI, nuclei (blue). Scale bar, 20 μm. **g** Quantification of p-S39-TRIM23-positive cells for the data shown in (**f**). **h** Top: Representative confocal microscopy images showing the colocalization of endogenous p-S39-TRIM23 with p-S172-TBK1 in HDFs that were either mock-treated or infected with WT HSV-1 or mutHSV-1 (MOI 0.3 for both) for 8 h, determined by Proximity Ligation Assay (PLA). Bottom: Quantification of the PLA signals for the data shown on top. PLA signal (magenta), HSV-1 ICP27 (green), nuclei (DAPI, blue). Scale bar, 20 μm. **i** S39 phosphorylation of TRIM23-FLAG in transiently transfected *TBK1* KO single cell clones (Cl-1 and Cl-2) and WT HEK293T cells, determined at 48 h post-transfection by IP with anti-FLAG and IB with anti-pS39-TRIM23. **j** S39 phosphorylation of FLAG-tagged TRIM23 WT or S39A in *TBK1* KO HEK293T cells that were co-transfected with either empty vector (−) or HA-TBK1, determined at 48 h post-transfection by IP with anti-FLAG and IB with anti-pS39-TRIM23. **k** GFP-LC3B puncta formation in *TBK1* KO and WT A549 cells that were transiently transfected with GFP-LC3B (green) and either empty vector or the indicated FLAG-tagged TRIM23 constructs (red), assessed at 48 h post-transfection by immunostaining with anti-FLAG followed by confocal microscopy analysis. DAPI, nuclei (blue), scale bar, 20 μm. **l** Quantification of GFP-LC3B puncta for the data shown in (**k**). All data (**a**–**l**) are representative of at least two independent experiments (mean ± SD of $n = 4$ blots (**d**), $n = 4$ biological replicates (**g**); mean ± SEM of $n = 49$, 48, 52, 51 and 49 cells respectively for the data plots from left to right (**h**); $n = 26$ cells (**l**). $^{**}p < 0.01$, $^{***}p < 0.001$, $^{****}p < 0.0001$ (two-tailed Student's t test (**d**, **g**), two-tailed Student's t test with Welch's correction (**h**, **l**). NS not significant. Source data are provided as a Source Data file.

in TRIM23 fail to activate autophagy in the brain and succumb more rapidly to HSV-1 infection, demonstrating a critical role for TRIM23 in controlling HSV-1 replication and neuropathogenesis. Our data further show that TRIM23-mediated autophagy restricts HSV-1 replication in a wide range of cell types (e.g., neuronal cells, epithelial cell lines, fibroblasts), and that this activity is independent of the antiviral type I IFN response. Furthermore, we discover that key to TRIM23 activation during HSV-1 infection is TBK1-mediated phosphorylation of its RING domain (at S39), which serves as an 'on/off' switch of its E3 ligase activity. Thus, our work identifies the TRIM23-TBK1 interconnection as an important orchestrator of HSV-1-induced autophagy. Of note, whereas TRIM23 reportedly positively regulates IFN induction in certain contexts[38], we observed an IFN-dampening role for TRIM23 in HSV-1 infection. How the dual activities of TRIM23 in autophagy vs. cytokine regulation are coordinated still needs to be defined mechanistically. It is tempting to speculate that whereas TRIM23's autophagy function aids in direct cellular clearance of HSV-1, its IFN-suppressive activity may curtail prolonged or chronic antiviral and proinflammatory gene induction. Autophagy plays a critical role in dampening cytokine responses[13,62,63]; however, the molecular mechanism(s) by which TRIM23 acts in this regulatory circuit are still unknown. Whether TRIM23's ability to bind and re-localize TBK1 to autophagosomes[30] plays a role in TRIM23's IFN-repressive role in HSV-1 infection, or alternatively, whether a distinct interactome defines TRIM23's impact on antiviral gene transcription, which could be cell type or stimulus dependent, warrants future work.

Our study discovers TRIM23 as a novel substrate of TBK1, a kinase that has recently emerged as a critical autophagy regulator[17,30,64–70] and is well-known to elicit IFN induction[6,71]. The signal transduction by many PRRs converges onto TBK1 which, once activated, drives IFNα/β gene expression[47]. However, the innate sensor(s) and upstream pathways that specifically activate TBK1-mediated autophagy during viral infection are not well defined. During infection with a specific virus, multiple different PRRs are activated, either in a temporal and/or cell type-specific manner. Through an RNAi screen of the major PRRs implicated in HSV-1 detection, we found that specifically cGAS activation prompts TRIM23 phosphorylation by TBK1 and ensuing autophagy to restrict HSV-1 infection. As TRIM23 mediates autophagy in response to several viruses[30], it would be interesting to explore if TBK1 regulates TRIM23 activation during other viral infections (other DNA viruses as well as RNA viruses), and if so, which PRR(s) drive TRIM23-TBK1-mediated autophagy in these contexts. Along these lines, since cGAS and its key adaptor STING also elicit autophagy in bacterial infection[72] and are activated in response to cellular perturbations (e.g., mitochondrial DNA leakage or aneuploidy)[6,73–76], future investigation should determine whether TRIM23 also mediates cGAS-induced autophagy in these contexts. More broadly, as other PRRs (e.g., certain NLRs or TLRs)[77,78] and diverse DAMPs (such as, mitochondrial DNA, ROS or ATP)[79,80] can elicit autophagy in a variety of disease conditions, it will be important to elucidate whether TBK1 and/or TRIM23 also regulate autophagic responses during these pathologies.

cGAS-STING activation elicits both canonical and non-canonical autophagy via multiple signaling pathways, which are likely initiated in a context- and/or cell type-dependent manner[6,12]. Specifically, STING induces unconventional autophagy or CASM that requires ATG5, the V-ATPase-ATG16L1 axis and the ion channel function of STING, but does not require other classical autophagy proteins (e.g., ULK1, BECLIN1, or the class III PI3K complex)[10,11,81]. For this STING-mediated 'autophagy-like' response, TBK1 and IRF3 are dispensable[11,56]. On the other hand, cGAS-STING stimulation induces classical autophagy via direct recruitment of TBK1 to STING leading to its phosphorylation (at S365), and this autophagic response is crucial for host defense against HSV-1 infection in vivo[82]. Classical autophagy following cGAS-STING and TBK1 activation is also essential for feedback regulation of the cGAS-mediated IFN response by facilitating the degradation of STING[13]. TBK1 plays an essential role in mediating p62 S403 phosphorylation downstream of cGAS-STING activation[11,13]. Our findings show that classical autophagy by cGAS stimulation or authentic HSV-1 infection requires TBK1's enzymatic activity which mediates direct phosphorylation of TRIM23 at S39. In support of this, fibroblasts from a HSE patient carrying a heterozygous kinase-defective, dominant-negative TBK1 mutation (G159A) show severely impaired autophagy upon dsDNA ligand stimulation or HSV-1 infection. The G159A mutant, when expressed in *TBK1* KO cells, fails to phosphorylate TRIM23 at S39 but efficiently interacts with TRIM23. Our data showing that TRIM23 only elicited autophagy in healthy control but not mutant TBK1 expressing fibroblasts, suggests that the defect in TBK1-TRIM23-induced autophagy likely contributed to the HSE seen in the mutant TBK1 heterozygous patient, besides the well-documented role of deficiency in the TLR3-IFN signaling axis. However, extensive additional experiments (e.g., in patient-derived neurons) are required to establish more directly the relative contribution of ablated TBK1-TRIM23-mediated autophagy to HSE. Along these lines, whether impaired TRIM23

https://doi.org/10.1038/s41467-025-59338-5

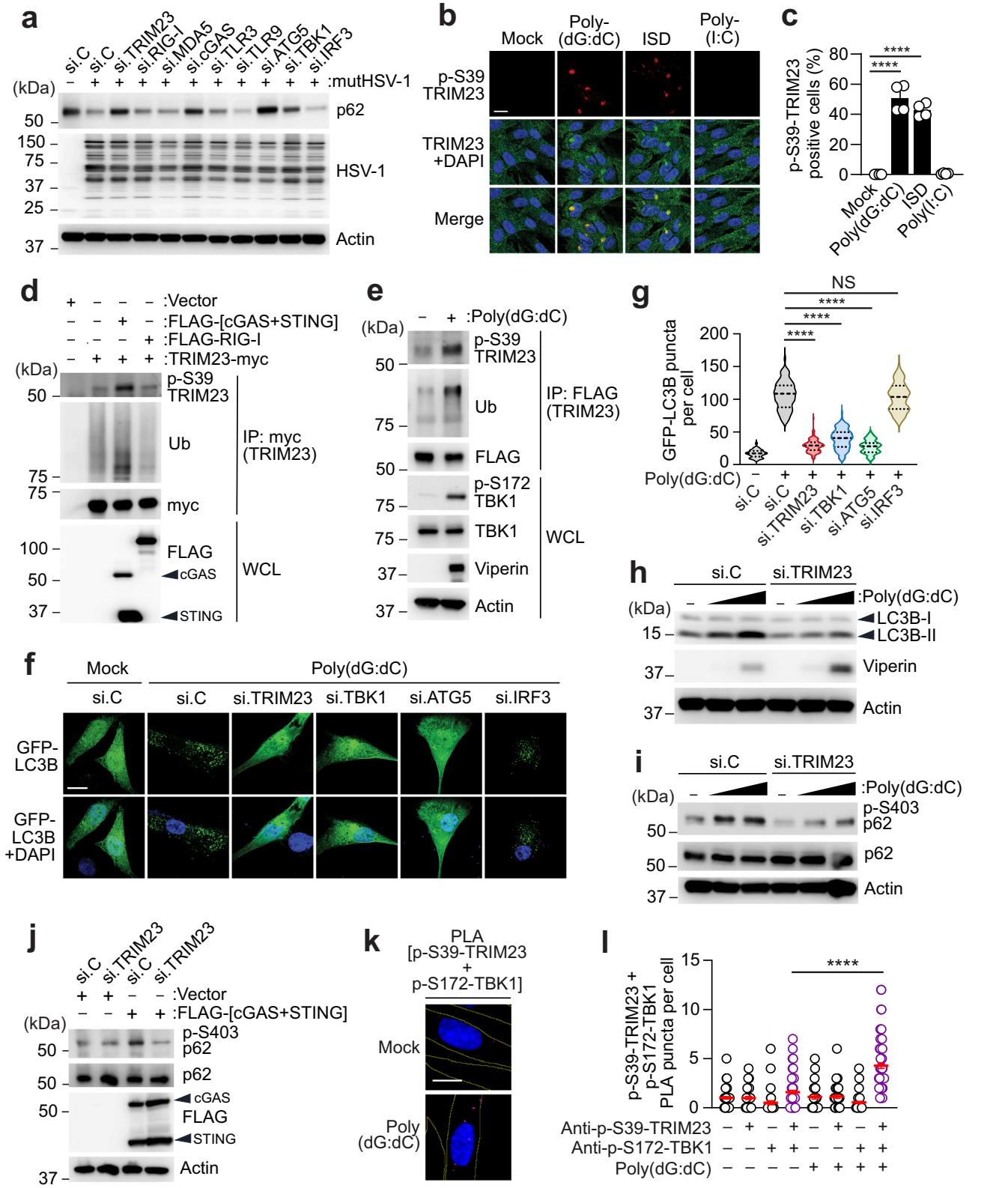

activation and autophagic control of HSV-1 infection contribute to the HSE of patients who carry other TBK1 mutations warrants future investigation.

Numerous viruses target TBK1 to escape type I IFN-mediated host immunity[83]. Given TBK1's emerging role in autophagy[64,65,69,84], combined with our work identifying TBK1 and TRIM23 as central molecules in HSV-1-induced autophagy, it is not surprising that HSV-1 has already evolved a mechanism to antagonize the TRIM23- and TBK1-mediated autophagy[85]. It will be important to determine whether also other viruses are equipped with strategies to commandeer TBK1's or TRIM23's autophagy function. Along these lines, cGAS and STING are the target of many viral antagonistic strategies[86]; as such, future studies should investigate how specific viral countermeasures affect autophagy induction by the cGAS-STING pathway.

Fig. 5 | cGAS signaling induces TRIM23 S39 phosphorylation via TBK1 to elicit autophagy. a Endogenous p62 protein abundance in the WCLs of HDFs that were transfected for 30 h with the indicated siRNAs and then either mock-treated (−) or infected with mutHSV-1 (MOI 10) for 20 h, determined by IB with anti-p62 and actin (loading control). WCLs were further immunoblotted with anti-HSV-1 to confirm efficient infection. **b** Endogenous TRIM23 S39 phosphorylation in HDFs that were either mock-treated or stimulated with poly(dG:dC)-LyoVec (3 μg/mL), ISD-LyoVec (5 μg/mL) or poly(I:C)-LyoVec (1.5 μg/mL) for 16 h, determined by immunostaining with the indicated antibodies and confocal microscopy analysis. DAPI, nuclei (blue). Scale bar, 20 μm. **c** Quantification of p-S39-TRIM23-positive cells for the data shown in (**b**). **d** S39 phosphorylation and ubiquitination of TRIM23-myc in transiently transfected HEK293T cells that also co-expressed empty vector, FLAG-cGAS and FLAG-STING, or FLAG-RIG-I, determined at 20 h post-transfection by IP with anti-myc and IB with anti-p-S39-TRIM23 or anti-Ub. **e** S39 phosphorylation and ubiquitination of FLAG-TRIM23 stably expressed in HDFs that were either mock-treated (−) or transfected with poly(dG:dC)-LyoVec (3 μg/mL) for 20 h, determined by IP with anti-FLAG and IB with anti-p-S39-TRIM23 or anti-Ub. **f** GFP-LC3B puncta formation in HDFs that were transfected for 24 h with the indicated siRNAs and then co-transfected for 12 h with GFP-LC3B (green) followed by mock treatment or stimulation with poly(dG:dC)-LyoVec (3 μg/mL) for 20 h, determined by confocal microscopy analysis. DAPI, nuclei (blue). Scale bar, 20 μm. **g** Quantification of GFP-LC3B puncta for the data shown in (**f**). **h** Endogenous LC3B-I-to-II conversion in HDFs that were transfected for 30 h with either si.C or si.TRIM23 and then stimulated with poly(dG:dC)-LyoVec (1 and 3 μg/mL) for 20 h, determined by IB with anti-LC3B and anti-actin (loading control). Viperin, an ISG, was included as a control to confirm efficient poly(dG:dC)-LyoVec stimulation. **i** Endogenous p62 phosphorylation (at S403) in HDFs that were transfected for 30 h with either si.C or si.TRIM23 and then stimulated with poly(dG:dC)-LyoVec (1 and 3 μg/mL) for 20 h, determined by IB with anti-p-S403-p62. In this assay, cells were treated with a combination of Pepstatin A and E64D (10 μg/mL each) for 4 h prior to harvesting to block autophagic flux. **j** Phosphorylation of endogenous p62 (at S403) in HEK293T cells that were transfected for 30 h with the indicated siRNAs and then co-transfected for 20 h with either empty vector or plasmids expressing FLAG-tagged cGAS and STING, determined in the WCLs by IB with the indicated antibodies. Autophagic flux was blocked as in (**i**). **k** Representative confocal microscopy images showing the colocalization of endogenous p-S39-TRIM23 with endogenous p-S172-TBK1 in HDFs that were either mock-treated or transfected with poly(dG:dC)-LyoVec (3 μg/mL) for 16 h, determined by PLA. PLA signal (magenta); nuclei (DAPI, blue). Scale bar, 20 μm. **l** Quantification of the PLA signals for the data shown in (**k**). All data (**a**–**l**) are representative of at least two independent experiments (mean ± SD of $n = 4$ biological replicates (**c**); mean ± SEM of $n = 120$ cells (**g**); $n = 60$, 42, 41, 92, 36, 44, 57, 92 cells respectively for the data plots from left to right (**l**). $^{*}p < 0.05$; $^{**}p < 0.01$; $^{***}p < 0.001$; $^{****}p < 0.0001$ (two-tailed Student's t test (**c**), or two-tailed Student's t test with Welch's correction (**g**, **l**). NS, not significant. Source data are provided as a Source Data file.

Our data show that TBK1 mediates TRIM23 phosphorylation in its N-terminal RING domain (at S39) which, likely through conformational changes, affects TRIM23's ubiquitin and/or E2 binding ability[43], or perhaps helps recruit other (accessory) proteins needed for effective E3 ligase activity. To our knowledge, this is the first phosphorylation-dependent 'on/off' switch of a TRIM E3 ligase. Of note, several other TRIM proteins harbor in their RING domain a Ser/Thr residue at the site equivalent to TRIM23 S39; this provides a mandate for exploring whether similar regulatory switches exist for other TRIM proteins or more broadly other RING E3 ligases.

The work presented here, combined with our previous findings[30], proposes a feed forward activation circuit in virus-induced autophagy driven by an intricate inter-regulation of TRIM23 and TBK1 (Supplementary Fig. 7d). First, RING phosphorylation at S39 by TBK1 licenses TRIM23's E3 ligase activity. TRIM23 auto-ubiquitination then stimulates GTPase cycling of its ARF domain and this, in turn, helps bound TBK1 to form higher-order assemblies, facilitating TBK1 trans-autophosphorylation and its translocation to autophagosomes where it induces phosphorylation of the autophagy receptor p62. The precise mechanism(s) that determine TBK1's activity towards TRIM23 and its autophagy function, including the role of specific PTMs in TBK1 itself in this process (of note, several PTMs are known to specifically regulate TBK1's IFN-inducing activity)[87–89] remain to be investigated.

In summary, this study broadens our understanding of cGAS-STING- and TBK1-mediated autophagy during virus infection and unveils a central role of TRIM23 in this process. Our work provides a mandate to comprehensively define the cellular machinery and additional factors involved in autophagy induction by the TBK1-TRIM23 complex, which is expected to reveal potential ways to therapeutically target this new axis in infectious diseases, inflammatory disorders, and autophagy-related pathologies.

Methods

Cells and viruses

Human embryonic kidney cells (HEK293T, CRL3216; ATCC), *ATG5* KO HEK293T cells[29], hTERT immortalized human dermal fibroblasts (HDFs, a gift from P. Hearing, Stony Brook University)[90], human adenocarcinoma cells (HeLa, CCL-2; ATCC), HeLa cells stably expressing GFP-LC3B (a gift from W.-X. Ding, University of Kansas Medical Center), and African green monkey kidney epithelial cells (Vero, CCL-81; ATCC) were cultured in Dulbecco's Modified Eagle Media (DMEM, 41965039; Gibco) supplemented with 10% (v/v) fetal bovine serum (FBS, 10270106; Gibco), 2 mM L-glutamine (25030081; Gibco), 1 mM sodium pyruvate (11360-070; Gibco) and 100 U ml^{-1} penicillin-streptomycin (Pen-Strep, 15140122; Gibco). STAT2-deficient (U6A) and parental human sarcoma cells (2fTGH, gifts from G. Stark, Cleveland Clinic Lerner Research Institute) were similarly cultured in DMEM supplemented with 10% (v/v) FBS, 2 mM L-glutamine and 100 U ml^{-1} Pen-Strep. Human neuroblastoma (SH-SY5Y, CRL-2266; ATCC) and mouse neuroblast (Neuro-2a, CCL-131; ATCC) cells were cultured in Modified Eagle Media (MEM, 11095-080; Gibco) supplemented with 10% (v/v) FBS, 1 mM sodium pyruvate, and 100 U ml^{-1} Pen-Strep. Human alveolar epithelial cells (A549, CCL-185; ATCC) were cultured in F12K media (21127-022; Gibco) supplemented with 10% (v/v) FBS and 100 U ml^{-1} Pen-Strep. Mouse embryonic fibroblasts (MEFs) from WT and *Ifnar1*$^{-/-}$ mice (provided by M.S. Diamond, Washington University in St. Louis) were cultured in DMEM supplemented with 10% (v/v) FBS, 100 U ml^{-1} Pen-Strep, 1 mM sodium pyruvate, and 2 mM L-glutamine. Immortalized fibroblasts from a human patient carrying the heterozygous TBK1 germline mutation (TBK1 p.G159A/WT) or from health control[58] were cultured in DMEM supplemented with 10% (v/v) FBS, 100 U ml^{-1} Pen-Strep, 1 mM sodium pyruvate, and 2 mM L-glutamine.

All cell cultures were maintained at 37 °C in a humidified 5% CO2 atmosphere. All commercially obtained cells were authenticated by the vendors and not further validated. Cell lines obtained from other groups, who have published these cells, were not further authenticated. The *TBK1* KO HEK293T, *TBK1* KO A549, and HDFs stably expressing FLAG-tagged human TRIM23 that were generated in this study were validated as described below and were cultured in the same way as the respective parental cell lines. All cell lines used in this study were regularly tested by PCR to ensure the absence of mycoplasma contamination.

HSV-1 (strain KOS) was provided by D. Knipe (Harvard University). Beclin-1-binding-deficient γ34.5 mutant recombinant HSV-1 (mutHSV-1) and the respective revertant virus[35] were provided by D. Leib (Dartmouth University). These viruses were propagated and tittered using Vero cells as described below.

Generation and genotyping of *Trim23* knockout mice

Trim23 knockout mice (*Trim23*$^{-/-}$)[34] were regenerated for the current study. Briefly, a targeting vector using pKO Scrambler 1903 vector

https://doi.org/10.1038/s41467-025-59338-5

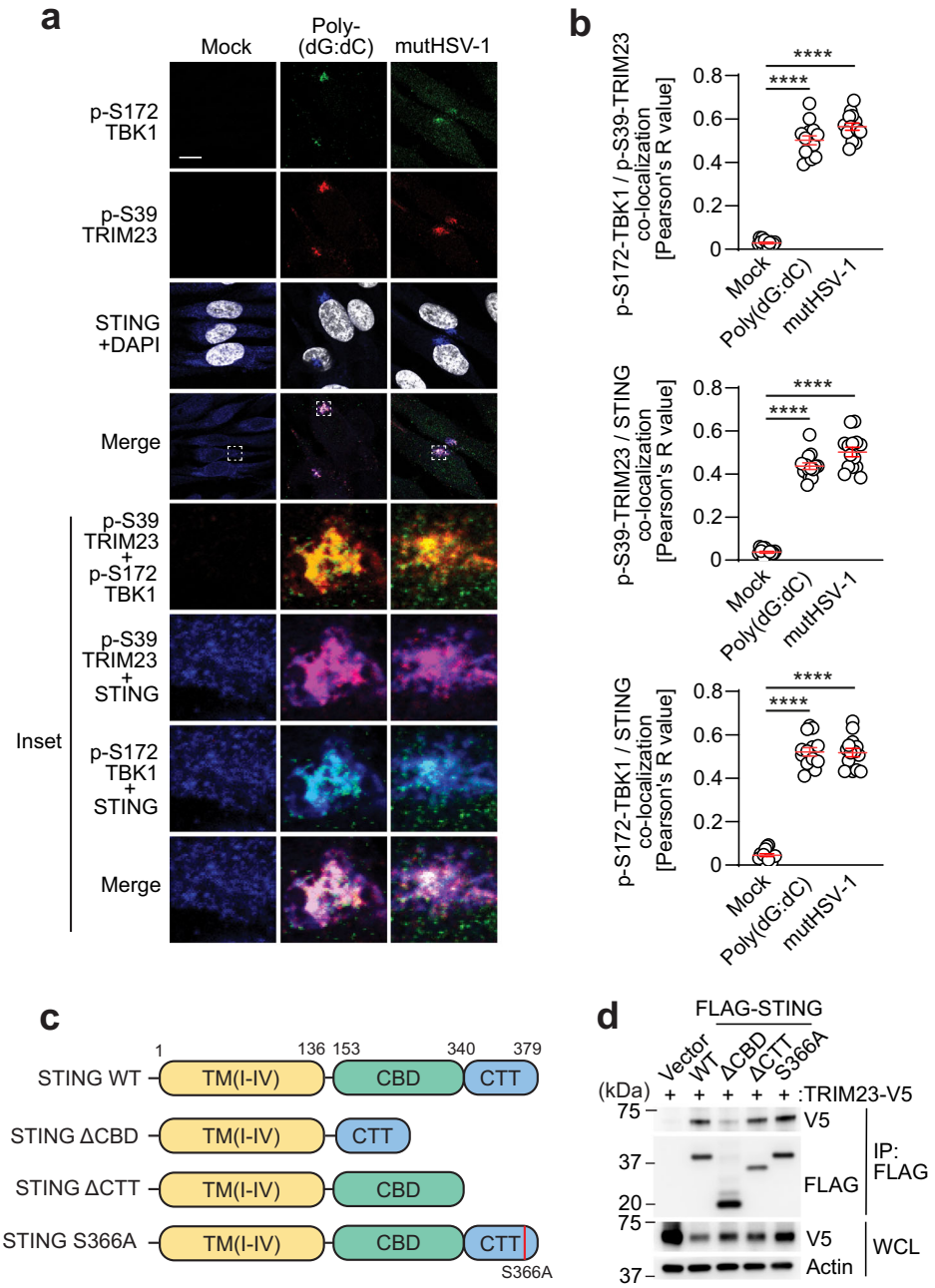

Fig. 6 | TRIM23, TBK1 and STING form a complex after HSV-1 infection or dsDNA stimulation. a Co-localization of endogenous p-S39-TRIM23, p-S172-TBK1 and STING in primary HDFs that were either mock-treated, infected with mutHSV-1 (MOI 5) or treated with poly(dG:dC)-LyoVec (3 μg/mL) for 16 h, determined by immunostaining with the indicated antibodies and confocal microscopy analysis. DAPI, nuclei (white). Scale bar, 20 μm. **b** Quantification of co-localization of the indicated proteins for the data shown in (**a**), determined by Pearson's correlation coefficient. **c** Schematic representation of the human STING domain organization as well as the mutant constructs used for the interaction mapping studies. **d** Binding of V5-tagged TRIM23 to FLAG-tagged STING WT and mutants in transiently transfected HEK293T cells, determined at 48 h post-transfection by IP with anti-FLAG and IB with anti-V5. Data (**a**, **b**, and **d**) are representative of at least two independent experiments (mean ± SEM of $n = 14$ cells (**b**)). $^{****}p < 0.0001$ (two-tailed Student's t test with Welch's correction). Source data are provided as a Source Data file.

(Stratagene) was prepared to delete a 2.8-kb DNA fragment that included a part of exon 2, intron 2, exon 3, and intron 3 of the mouse *Trim23* gene. Neomycin resistance and thymidine kinase genes in the targeting vector were used, respectively, as positive and negative selection markers of homologous recombination. The unique Sal I restriction enzyme site was used to linearize the pKO vector before electroporation into embryonic stem (ES) cells. Positive ES clones were selected using G418 (A1720, MilliporeSigma) and ganciclovir (G2536, MilliporeSigma). Chimeric mice were generated by microinjecting ES cells (129/SvJ) into blastocysts from C57BL/6 J mice. Heterozygous (*Trim23*$^{+/-}$) mice were used for breeding to generate homozygous (*Trim23*$^{-/-}$), heterozygous (*Trim23*$^{+/-}$), and wild-type (*Trim23*$^{+/+}$) animals. Genotypes of the mice were confirmed by PCR[34]. A set of one forward primer and two reverse primers (Supplementary Table 1) were used for PCR amplification of the *Trim23* genomic DNA fragment. A 2.4-kb wild-type *Trim23* fragment from the wild-type allele was generated using F1-G and R1-G primers. A 2.1-kb mutant *Trim23* fragment from the neomycin-disrupted allele was generated using F1-G and R-NEO primers. *Trim23*$^{-/-}$ mice were backcrossed 10 times using C57BL/6 J mice (Jackson laboratories, stock #000664).

https://doi.org/10.1038/s41467-025-59338-5

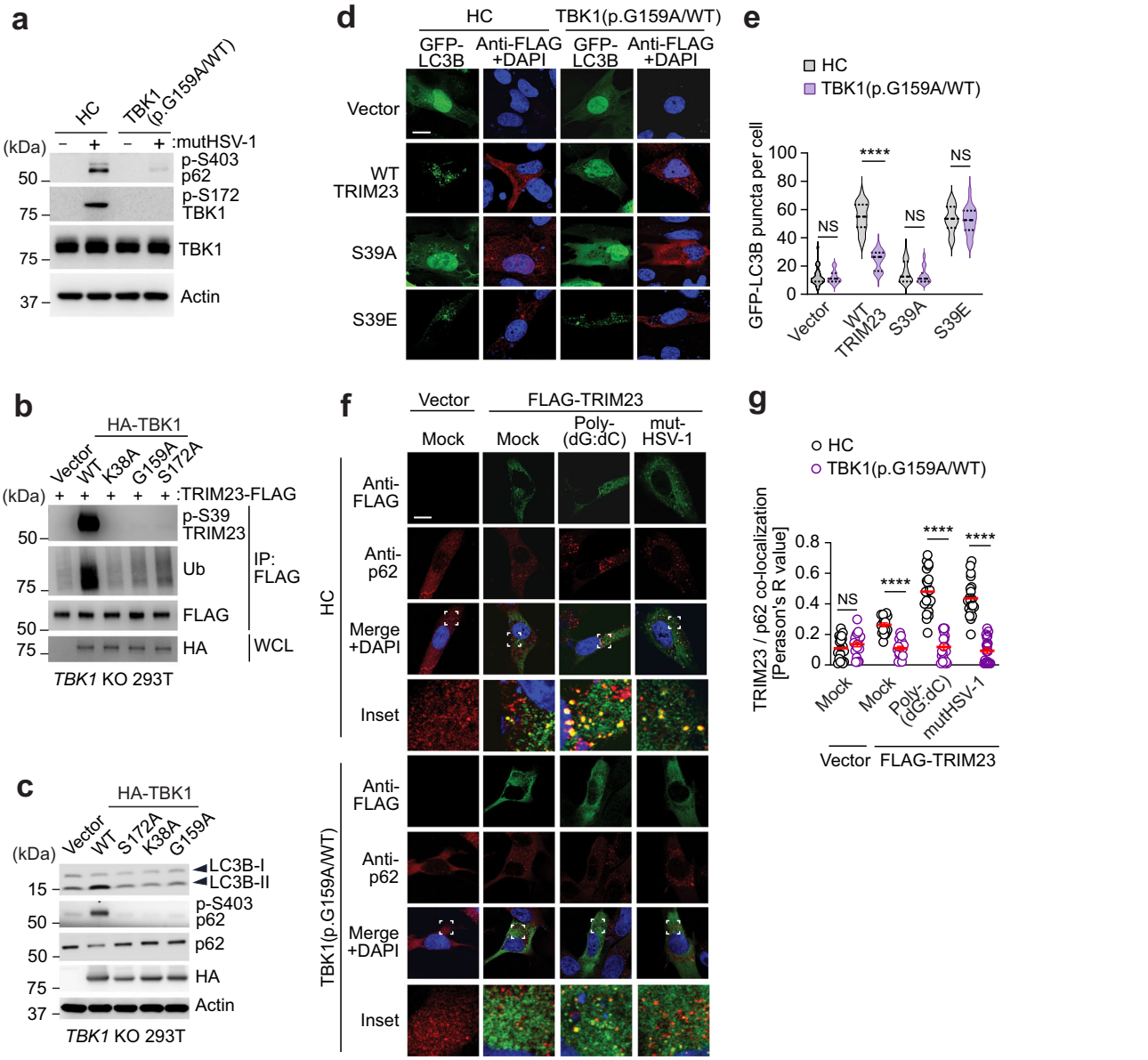

Fig. 7 | HSE patient fibroblasts carrying a TBK1 'null' mutation exhibit impaired TRIM23 activation. a Phosphorylation of endogenous p62 (at S403) and TBK1 (at S172) in the WCLs of either healthy control (HC) or patient fibroblasts carrying the heterozygous TBK1 mutation G159A (TBK1(p.G159A/WT)) that were either mock-treated (−) or infected with mutHSV1 (MOI 1) for 16 h, determined by IB using the indicated antibodies. **b** S39 phosphorylation and ubiquitination of TRIM23-FLAG in transiently transfected *TBK1* KO HEK293T cells that were reconstituted with HA-tagged TBK1 WT or mutants, determined at 48 h post-transfection by IP with anti-FLAG and IB with the indicated antibodies. **c** Endogenous LC3B-I-to-II conversion and p62 phosphorylation (at S403) in *TBK1* KO HEK293T cells that were transiently transfected with HA-tagged TBK1 WT or mutants, determined at 24 h post-transfection in the WCLs by IB with the indicated antibodies. **d** GFP-LC3B puncta formation in HC or patient fibroblasts that were transiently transfected with GFP-LC3B (green) together with either empty vector or the indicated FLAG-tagged TRIM23 constructs (red), assessed at 24 h post-transfection by immunostaining with anti-FLAG and confocal microscopy analysis. DAPI, nuclei (blue). Scale bar, 20 μm. **e** Quantification of GFP-LC3B puncta for the data shown in (**d**). **f** Colocalization of FLAG-TRIM23 (green) and endogenous p62 (red) in HC and patient fibroblasts that were transfected with empty vector (control) or FLAG-tagged TRIM23 for 20 h and then either mock-treated, transfected with poly(dG:dC)-LyoVec (3 μg/mL) or infected with mutHSV-1 (MOI 5) for 20 h, determined by confocal microscopy after immunostaining with the indicated antibodies. DAPI, nuclei (blue). Scale bar, 20 μm. **g** Quantification of FLAG-TRIM23 colocalization with p62 for the data shown in (**f**), determined by Pearson's correlation coefficient. All data (**a**–**g**) are representative of at least two independent experiments (mean ± SEM of $n = 26$ cells (**e**), $n = 20$ cells (**g**). ****$p < 0.0001$ (two-tailed Student's t test with Welch's correction (**e**, **g**). NS, not significant. Source data are provided as a Source Data file.

Trim23$^{-/-}$ mice and WT (*Trim23*$^{+/+}$) controls (both in C57BL/6J background) were co-housed and maintained in a specific pathogen-free barrier facility (room temperature of 68-79 °F and humidity of 30-70%) with a 12 h dark/light cycle and with *ad libitum* access to standard diet and water at the animal facility of The University of Chicago or the Cleveland Clinic Florida Research and Innovation Center (CC-FRIC). All mice used in the current study were in good health status and not involved in any other experiments or procedures. All mice were handled according to institutional guidelines under protocols approved by the Institutional Animal Care and Use Committee of The University of Chicago or CC-FRIC.

Plasmids

The plasmid expressing human TRIM23-myc-FLAG (pCMV6 backbone)[30] was used as a template to introduce specific point mutations by site-directed mutagenesis to generate the TRIM23

mutants S39A, S39D, and S39E. TRIM23 with a C-terminal myc tag or N-terminal FLAG tag was generated by subcloning hTRIM23 cDNA into the pLVX-IRES-puro vector using *SpeI* and *NotI* restriction sites. 3X-HA tagged human TBK1 was generated by subcloning it into the pcDNA3.1 vector with a 3X-HA tag using FLAG-TBK1[30] as a template. The TBK1 single-point mutants S172A, K38A, and G159A were generated by overlapping PCR. The plasmids expressing human FLAG-Rab5a[30], HA-Ub(K27only)[30], TRIM23 C34A-myc-FLAG[30], TRIM23 K458I-myc-FLAG[30], TRIM23 ΔRING-myc-FLAG[30], TRIM23 ΔARF-myc-FLAG[30], FLAG-RIG-I[91], FLAG-MDA5[91] and FLAG-MAVS[91] were described elsewhere. The plasmids expressing human FLAG-cGAS, FLAG-STING, FLAG-IRF3-5D and HA-IKKβ were obtained as gifts from J. U. Jung (Cleveland Clinic Lerner Research Institute). The FLAG-tagged STING mutants ΔCBD, ΔCTT, and S366A were generated using FLAG-STING as a template. The sequence of all constructs was confirmed by Sanger sequencing.

In vivo studies

All mouse studies were conducted in the animal BSL-2 (ABSL-2) facilities at The University of Chicago or the Cleveland Clinic Florida Research and Innovation Center strictly following the procedures and guidelines approved by the respective Institutional Animal Care and Use Committees (IACUC) that are in accordance with the National Institutes of Health Guide for the Care and Use of Laboratory Animals.

Eight-week-old *Trim23*$^{+/+}$ and *Trim23*$^{-/-}$ mice of both sexes (sex-matched across treatments) were anesthetized and intracranially inoculated with mutHSV-1 or revertant virus at the indicated MOIs[35,92]. For survival studies, infected mice were monitored daily until day 14 post-infection for morbidity/clinical signs and euthanized when humane endpoint criteria were reached as defined by the Institutional Animal Care and Use Committee guidelines. HSV-1 burden in the brains of infected mice was analyzed by plaque forming assay as described below. Expression levels of transcripts of HSV-1 genes and host antiviral genes in the brains of HSV-1-infected mice were determined by RT-qPCR as detailed below. Expression of HSV-1 antigen and autophagy markers in the brains of infected mice were assessed by immunohistochemistry of brain sections and/or by immunoblotting of brain lysates as described below.

Generation of CRISPR TBK1 knockout cells and TRIM23 stably expressing cells

To generate *TBK1* KO A549 and HEK293T cells, gene-specific guide RNAs (gRNAs)[93] or non-targeting control gRNA[94] (Supplementary Table 1) were cloned into the pSicoR-CRISPR-PuroR vector at the BsmB1 restriction site[94] and sequenced to confirm correct insertion of gRNAs. gRNA-encoding plasmids, together with the third-generation lentivirus packaging plasmids pmDC gag/pol, pRSV rev, and pmDC VSV-G (kindly provided by J. U. Jung, Cleveland Clinic Lerner Research Institute) were then transfected into HEK293T cells to generate lentiviral particles[95]. Transduction of target cells was performed in 6-well plates and, at 48 h post-transduction, the cells were subjected to selection in culture media containing 2 μg/mL puromycin (ant-pr-5; InvivoGen). Single clones of puromycin-resistant cells were sorted by FACS. The clonal *TBK1* KO and control cells were validated by IB analysis of TBK1 protein expression as described below.

HDF cells stably expressing FLAG-TRIM23 (cloned into pLVX-IRES-Puro vector with N-terminal FLAG tag (PT4063-5, 632183; Takara Bio) were generated by lentiviral transduction, followed by selection with puromycin (2 μg ml^{-1}) at 48 h post-transduction. Stable expression of FLAG-TRIM23 in these cells was confirmed by IB analysis of WCLs using an anti-FLAG antibody as described below.

Transfection and gene silencing

Transient DNA plasmid transfections were performed using linear polyethylenimine (PEI, 00618; Polysciences) prepared as 1 mg/mL solution (in 10 mM Tris, pH 6.8)[96] or by using commercially obtained transfection reagents (i.e., Lipofectamine LTX and PLUS reagent (15338100; Thermo Scientific), Lipofectamine 2000 (11668019; Thermo Fischer), TransIT-X2 (MIR 6005; Mirus bio), or TransIT-HelaMONSTER (MIR 2900; Mirus bio)) following the manufacturers' instructions.

Transient gene silencing in cells was achieved by using predesigned and validated gene-specific siGENOME SMARTpool siRNAs that were commercially obtained (Horizon Discovery). The following siRNAs were used: human TRIM23 (M-006523-00-0020), human ATG5 (M-004374-04-0010), human STK38 (M-004674-01-0005), human ATR (M-003202-05-0005), human AMPKα2 (M-005361-02-0005), human MAP3K5 (M-003584-02-0005), human LRRK1 (M-005320-02-0005), human IKKε (M-003723-02-0005), human TBK1 (M-003788-02-0010), human RIPK2 (M-003602-02-0005), human ROCK1 (M-003536-02-0005), human IKKβ (M-003503-03-0005), human PINK1 (M-004030-02-0005), human RIG-I (M-012511-01-0020), human MDA5 (M-013041-00-0005), human cGAS (M-015607-01-0010), human STING (M-024333-00-0010) human TLR3 (M-007745-00-0020), human TLR9 (M-004066-01-0010), human IRF3 (M-006875-02-0020), mouse TRIM23 (M-048442-01-0010), non-targeting control siRNA (D-001206-14-05; D-001210-03-05). siRNAs (at a final concentration of 80 nM) were reverse-transfected into target cells (seeded into 12- or 6-well plates) according to the manufacturer's instructions using Lipofectamine RNAiMAX (13778075; Thermo Scientific). After transfection, cells were infected with virus or stimulated as indicated in the respective figure legends. Knockdown efficiency was determined at the indicated times after siRNA transfection by measuring the transcripts of the respective gene by RT-qPCR using gene-specific predesigned PrimeTime qPCR Probe Assays (Integrated DNA Technologies) as described below.

Cell lysis, immunoprecipitation and cell treatments

Cell harvesting, cell lysis, and co-immunoprecipitation of proteins were performed following our published methods[30,96]. Briefly, cell lysis was carried out using Nonidet P-40 (NP-40, 1%) lysis buffer (50 mM HEPES pH 7.4, 150 mM NaCl, 1% (v/v) NP-40, 1 mM EDTA) or radioimmunoprecipitation assay (RIPA) buffer (50 mM Tris-HCl; pH 7.4, 150 mM NaCl, 1% (v/v) NP-40, 0.5% (w/v) deoxycholic acid, and 0.1% (w/v) SDS) containing protease inhibitor (P2714; MilliporeSigma) and phosphatase inhibitor (P0044; MilliporeSigma) cocktails. For immunoprecipitation, cleared cell lysates were incubated at 4 °C for 6 to 16 h either with magnetic or agarose beads pre-conjugated with antibody against the protein tag, or with primary antibodies (1-2 μg/mL) raised against the specific protein or protein tag. Immunoprecipitation of protein from cell lysates using specific primary antibodies was achieved by coupling to protein A, G, or A/G conjugated agarose or magnetic beads for an additional 2 h at 4 °C. Beads were extensively washed with NP-40 or RIPA buffer, and the immunoprecipitated proteins were eluted in 1X Laemmli SDS sample buffer (S3401; MilliporeSigma) by heating samples at 95 °C for 5 min.

For the detection of TRIM23 phosphorylation at S39, calyculin A (PHZ1044; Invitrogen) at a concentration of 50 nM was added to the cells 30 min pre-harvest and, additionally, also to the cell lysis buffer. Cells were treated with a combination of Pepstatin A (P5318; MilliporeSigma) and E64D (E8640; MilliporeSigma) (used at 10 μg/mL for 3–4 h) to block autophagic flux in the experiments shown in Fig. 3b, d 4k, 5i, j, and 7d. Bafilomycin A1 (54645, Cell Signaling Technology) and MG132 (M8699, MilliporeSigma) were used to block lysosomal or proteasomal degradation of proteins, respectively. Rapamycin (R8781; MilliporeSigma) at a concentration of 1-3 μM was used as a positive control to induce autophagy. Cells were treated with BX795 (204001; MilliporeSigma) as indicated in the respective figure legends to inhibit TBK1.

Immunoblotting and antibodies

Immunoprecipitated protein samples or WCLs were resolved on 7–12% Bis-Tris SDS-PAGE gels, transferred onto polyvinylidene difluoride (PVDF) membranes (1620177; Bio-Rad), blocked in 5% (w/v) skim milk (902887; MP Biomedicals) or 5% (w/v) BSA (A7030; MilliporeSigma), probed with the specified antibodies, and proteins on the membranes were visualized following our published methods using the Super-Signal West Pico PLUS or Femto chemiluminescence reagents (both purchased from Thermo Fisher Scientific) on an ImageQuant LAS 4000 Chemiluminescent Image Analyzer (General Electric)[96,97]. Primary antibodies that were used for IB and theirs dilutions include: anti-FLAG (1:2,000, F1804; MilliporeSigma), anti-myc (1:2,000, 2276S; Cell Signaling Technology), anti-HA (1:2,000, H9658; MilliporeSigma), anti-β-actin (1:5,000, A5441; MilliporeSigma), anti-p-S39-TRIM23 (custom made by GenScript, 1:500), anti-TBK1 (1:1,000, 3504S; Cell Signaling Technology), anti-p-S172-TBK1 (1:1,000, 5483S; Cell Signaling Technology), anti-LC3B (1:2,000, CAC-CTB-LC3-1-50; Cosmo Bio), anti-p62 (1:2,000, GP62-C; Progen), anti-p-S403-p62 (1:1,000, 39786; Cell Signaling Technology); anti-IFIT1 (1:1,000, 14769; Cell Signaling Technology), anti-viperin (1:1,000, 13996S; Cell Signaling Technology), anti-ISG15 (1:1000, sc-166755; Santa Cruz); anti-ubiquitin (1:1,000, sc-8017; Santa Cruz), and anti-HSV-1 (1:1,000, B0114; Dako). Secondary (HRP-linked) antibodies that were used for IB as well as their dilutions are: anti-mouse IgG (1:4000, 7076; Cell Signaling Technology); anti-rabbit IgG (1:4000, 7074; Cell Signaling Technology); light chain specific anti-rabbit IgG (1:4000, 211-032-171; Jackson Immunoresearch); light chain specific anti-mouse IgG (1:5000, 115-035-174; Jackson Immunoresearch); anti-guinea pig IgG (1:4000; PA128597; Invitrogen). Monoclonal anti-IFNAR2 antibody (clone MMHAR-2) was obtained from PBL Assay Science.

Mass spectrometry analysis

To identify post-translational modifications of TRIM23, twelve 10 cm-dishes of HEK293T cells (~5×10^6 cells/dish) were transfected with either empty vector or FLAG-tagged TRIM23. At 48 h post-transfection, cells were harvested and washed with PBS and lysed with 1% (v/v) NP40 lysis buffer containing protease inhibitor (P2714; Millipore Sigma) and phosphatase inhibitor (P0044; Millipore Sigma) cocktails. Lysates were cleared by centrifugation at 21,000 × *g* for 20 min at 4 °C, and supernatants were incubated with anti-FLAG M2 magnetic beads (M8823; Millipore Sigma) at 4 °C for 6 h. Pulldown samples were washed harshly with RIPA buffer (1 M NaCl, 1% (v/v) NP-40, 1% (w/v) deoxycholic acid, 0.01% (w/v) SDS, 20 mM Tris (pH 8.0)) and resolved by SDS-PAGE. The gel was stained with Coomassie blue followed by destaining with UltraPure water (10977-015; Invitrogen). The band corresponding to the size of TRIM23-FLAG was excised and subjected to ion-trap MS analysis at the Harvard Taplin Biological Mass Spectrometry Facility, Boston.

Immunohistochemistry

Immunohistochemistry of mid-sagittal brain sections of PFA-fixed paraffin embedded murine brain tissue samples that were collected from mutHSV-1- or mock-infected WT and *Trim23*$^{-/-}$ mice were performed at the University of Chicago Human Tissue Resource Center Core Facility using anti-p62 (1:100, GP62-C; Progen) and anti-HSV-1 (1:100, B0144; Dako).

RNA isolation and RT-qPCR analysis

RNA isolation and RT-qPCR analysis were performed following our published methods[96] using the SuperScript III Platinum One-Step RT-qPCR Kit (11732088; Invitrogen) and commercially available predesigned PrimeTime qPCR Probe Assays (Integrated DNA Technologies). The following primers were used: human GAPDH (Hs.PT.39a.22214836), human IFNB1 (Hs.PT.58.39481063.g), human TNFα (Hs.PT.58.45380900), human IFIT1 (Hs.PT.56a.20769090.g), human TRIM23 (Hs.PT.56a.19904019), human ATG5 (Hs.PT.58.2898629), human STK38 (Hs.PT.58.5035126), human ATR (Hs.PT.56a.39957055), human AMPKα2 (Hs.PT.58.3219579), human MAP3K5 (Hs.PT.58.2843674), human LRRK1 (Hs.PT.58.4447835), human IKKε (Hs.PT.58.25670557), human TBK1 (Hs.PT.58.21238234), human RIPK2 (Hs.PT.58.95241), human ROCK1 (Hs.PT.58.39473758), human IKKβ (Hs.PT.58.40427794), human PINK1 (Hs.PT.58.27157402), human RIG-I (Hs.PT.58.4273674), human MDA5 (Hs.PT.58.1224165), human CGAS (Hs.PT.58.20682405), human TLR3 (Hs.PT.58.15632456), human TLR9 (Hs.PT.58.40576968), human IRF3 (Hs.PT.58.15632456), mouse GAPDH (Mm.PT.39a.1), mouse IFNB1 (Mm.PT.58.30132453.g), and mouse OAS1 (Mm.PT.58.30459792). HSV-1 replication was assessed by RT-qPCR using gene-specific primers and probes for viral *ICP-0, ICP-8, UL36* and *gB* genes (Supplementary Table 1)[53]. The relative mRNA expression of the gene of interest was calculated by using the comparative threshold ($\Delta\Delta C_t$) method and expressed relative to the values for respective control cells. Gene expression levels were normalized to cellular *GAPDH* expression.

Virus infection and plaque assay

Infection of the indicated cells with HSV-1 (WT or mutant) was performed in DMEM supplemented with 10% FBS, 2 mM glutamine, and 1% (v/v) Pen-Strep at the indicated MOIs (described in the respective figures or figure legends) for 1 h at 37 °C, after which the virus inoculum was replaced with fresh supplemented complete culture medium[98]. HSV-1 titering was performed by standard plaque assay on Vero cells[30]. For determining HSV-1 titers in mouse brain, brain tissues were homogenized in DMEM containing 2% (v/v) FBS, and the supernatants obtained after centrifugation of homogenates were subjected to standard plaque assay on Vero cells[30].

Confocal microscopy

Cells were cultured and infected, stimulated and/or transfected on 12 mm-cover slips. At the indicated times, cells were fixed with 4% (w/v) paraformaldehyde (sc-281692; Santa Cruz) and permeabilized with 0.2% Triton X-100 (T8787; MilliporeSigma) in PBS (14190-144; Gibco)[99]. Cells were then blocked with PBS containing 0.05% (v/v) Triton-X-100 and 2% (w/v) BSA (in PBS, A7030; MilliporeSigma) for 1 h at room temperature. After washing with PBS, cells were incubated overnight with primary antibodies (i.e., anti-FLAG (1:200, F1804; Millipore Sigma), anti-p62 (1:200, GP62-C; Progen), anti-HSV-1/2 ICP27 (1:300, sc-69806; Santa Cruz), anti-TRIM23 (1:150, sc-393923; Santa Cruz), anti-p-S39-TRIM23 (1:1000, custom made by GenScript), anti-p-S172-TBK1 (1:500, 558397; BD Biosciences), and anti-STING (1:500, AF6516; R&D Systems) diluted in PBS containing 1% (w/v) BSA at 4 °C on a rocking platform. Cells were washed three times with PBS containing 0.25% (v/v) Tween-20 and then incubated with secondary antibodies conjugated to Alexa Fluor 488 (1:500, A21202; Invitrogen), Alexa Fluor 555 (1:500, A21435; Invitrogen) or Alexa Fluor 633 (1:500, A21050; Invitrogen). Cells were washed three times with PBS containing 0.25% (v/v) Tween-20 (P1379; MilliporeSigma), mounted in Prolong Gold Antifade mountant after DAPI staining (P36934; Invitrogen), and imaged using a Leica Stellaris 8 confocal microscope or a Leica SP8 system.

In vitro kinase assay

In vitro kinase assay was performed using commercially obtained purified human recombinant TRIM23 (harboring an N-terminal GST tag) and a commercial TBK1 kinase Enzyme System kit (V3991; Promega) that contains human recombinant full-length TBK1 (purified from Sf9 cells). Briefly, kinase (50 to 200 ng of TBK1, V3991; Promega) and substrate (0.5 μg of TRIM23, H00000373-P01, Abnova) were co-incubated in a 20 μL reaction mixture containing kinase buffer (40 mM Tris pH 7.5, 20 mM MgCl2, 0.1 mg/mL BSA and 50 μM DTT) and ATP (1 mM, A6559; MilliporeSigma) for 1 h at room temperature.

The reaction was stopped by heating samples in 1X Laemmli SDS sample buffer (S3401; Millipore Sigma) at 95 °C for 5 min. Phosphorylation of TRIM23 at S39 was assessed by immunoblotting as described above.

In vitro GTPase assay

For the assessment of GTPase activity, HEK293T cells were transiently transfected with FLAG-tagged TRIM23 WT and mutants, or Rab5a (positive control) using PEI. Alternatively, HEK293T *ATG5* KO cells were transfected using PEI with FLAG-tagged TRIM23 together with either cGAS and STING or empty vector, or with Rab5a (positive control). At 24 h (HEK293T *ATG5* KO) or 48 h (HEK293T) post-transfection, cells were harvested and lysed in GTPase lysis buffer (150 mM NaCl, 5 mM EDTA, 1% (v/v) Triton X-100, 50 mM HEPES (pH 7.4) and protease inhibitor cocktail). Cell debris were pelleted by centrifugation at 21,000 x g for 20 min at 4 °C, and the protein concentration in the cleared WCLs was determined using the Pierce Rapid Gold BCA Protein Assay Kit (A53226; Thermo Fisher). WCLs with normalized protein concentrations were then incubated with magnetic beads conjugated with anti-FLAG M2 antibody (M8823; Millipore Sigma) on a rotary shaker for 4 h at 4 °C. After incubation, supernatants were removed from the beads using a magnetic rack, and the beads were extensively washed three times with washing buffer I (500 mM NaCl, 5 mM EDTA, 5 mM $MgCl_2$, 1% (v/v) Triton X-100, 50 mM HEPES (pH 7.4) and protease inhibitor cocktail) and twice with washing buffer II (100 mM NaCl, 5 mM EDTA, 5 mM $MgCl_2$, 1% (v/v) Triton X-100, 50 mM HEPES (pH 7.4) and protease inhibitor cocktail). Subsequently, the GTPase activity was determined by a GTPase-Glo assay (V7681; Promega) following the manufacturer's recommendations. In brief, GEF assay buffer (containing 1 mM DTT and 0.1 mg/mL cardiolipin) was added to the beads, and incubation with 2X GTP solution was carried out at 37 °C for 16 h. Following this, the GTPase-Glo reagent and the detection reagent were added, and luminescence detection was performed using an Orion II microplate Luminometer (Berthold Detection Systems).

Proximity ligation assay

HDF cells were seeded onto 12 mm glass cover slips and cultured for 24 h before stimulation or infection as indicated in the respective figure legends. At the indicated times, the cells were harvested and fixed with 3.7% (w/v) PFA (in PBS, sc-281692; Santa Cruz) for 10 min, followed by permeabilization in 0.5% (v/v) Triton X-100 (T8787; MilliporeSigma) for 7 min and blocking with 5% (w/v) BSA (in PBS, A7030; MilliporeSigma) for 1 h. Cells were then incubated with primary antibody for overnight at 4 °C. The following primary antibodies were used: anti-p-S39-TRIM23 (1:200, custom made by GenScript), anti-ATG16 (1:200, sc-393274; Santa Cruz), anti-GM130 (1:100, sc55591; Santa Cruz), and anti-p-S172-TBK1 (1:200, 558397; BD Bioscience). PLA staining was performed using the Duolink PLA Fluorescence Protocol (DUO92002, DUO92004; MilliporeSigma) following the manufacturer's instructions and our published methods[100].

Bioinformatic analysis and structural modeling

Kinase prediction for the TRIM23 pS39 site was performed using GPS3[101], PKIS[102], and PhosphoNet (http://www.phosphonet.ca). A 15 amino acid sequence surrounding the pS39 site (i.e., $_{32}$GVCEDVFSLQGDKVP$_{46}$) was used for kinase prediction. Candidate kinases were selected for the targeted RNAi screen based on their prediction score values, cellular localizations, and/or reported roles in autophagy. Amino acid sequence alignments were done by using ClustalW (https://www.genome.jp/tools-bin/clustalw).

Structural modeling of the TRIM23 RING dimer[43] bound to E2 enzyme and ubiquitin was performed and illustrated using PyMOL (Schrodinger, Inc.).

Statistical analysis

Data are presented as mean ± SD or mean ± SEM as indicated in the respective figure legends. Data were analyzed using Prism software version 10 (GraphPad). Unless otherwise stated, an unpaired two-tailed Student's *t*-test ($p < 0.05$ was considered statistically significant) was used for statistical analysis. An unpaired two-tailed Student's *t*-test with Welch's correction was used for the statistical analysis of all data with a sample size of $n \geq 6$. For all statistical analyses, significant differences are denoted by $^{*}p < 0.05$, $^{**}p < 0.01$, $^{***}p < 0.001$ and $^{****}p < 0.0001$. Pre-specified effect sizes were not assumed and generally three biological replicates (n) for each condition were used, unless indicated otherwise. Data were reproduced in independent experiments as indicated in the legend for each figure.

Reporting summary

Further information on research design is available in the Nature Portfolio Reporting Summary linked to this article.

Data availability

All data are included in the article and Supplementary Information or available upon request from the corresponding author, as are unique reagents used in this article. The raw numbers for charts and graphs are available in the Source Data file. Source data are provided with this paper.

References

1. Klionsky, D. J. et al. Autophagy in major human diseases. *EMBO J.* **40**, e108863 (2021).
2. Lee, H. K. & Iwasaki, A. Autophagy and antiviral immunity. *Curr. Opin. Immunol.* **20**, 23–29 (2008).
3. Mizushima, N. & Levine, B. Autophagy in human diseases. *N. Engl. J. Med* **383**, 1564–1576 (2020).
4. Choi, Y., Bowman, J. W. & Jung, J. U. Autophagy during viral infection - a double-edged sword. *Nat. Rev. Microbiol* **16**, 341–354 (2018).
5. Ablasser, A. & Chen, Z. J. cGAS in action: Expanding roles in immunity and inflammation. *Science* **363**, eaat8657 (2019).
6. Motwani, M., Pesiridis, S. & Fitzgerald, K. A. DNA sensing by the cGAS-STING pathway in health and disease. *Nat. Rev. Genet*. **20**, 657–674 (2019).
7. Watson, R. O. et al. The cytosolic sensor cGAS detects mycobacterium tuberculosis DNA to induce type I interferons and activate autophagy. *Cell Host Microbe* **17**, 811–819 (2015).
8. Mackenzie, K. J. et al. cGAS surveillance of micronuclei links genome instability to innate immunity. *Nature* **548**, 461–465 (2017).
9. Nassour, J. et al. Autophagic cell death restricts chromosomal instability during replicative crisis. *Nature* **565**, 659–663 (2019).
10. Fischer, T. D., Wang, C., Padman, B. S., Lazarou, M. & Youle, R. J. STING induces LC3B lipidation onto single-membrane vesicles via the V-ATPase and ATG16L1-WD40 domain. *J. Cell Biol.* **219**, e202009128 (2020).
11. Gui, X. et al. Autophagy induction via STING trafficking is a primordial function of the cGAS pathway. *Nature* **567**, 262–266 (2019).
12. Lu, Q., Chen, Y., Li, J., Zhu, F. & Zheng, Z. Crosstalk between cGAS-STING pathway and autophagy in cancer immunity. *Front Immunol.* **14**, 1139595 (2023).
13. Prabakaran, T. et al. Attenuation of cGAS-STING signaling is mediated by a p62/SQSTM1-dependent autophagy pathway activated by TBK1. *EMBO J* **37**, e97858 (2018).
14. Schmid, M. et al. The interplay between autophagy and cGAS-STING signaling and its implications for cancer. *Front Immunol.* **15**, 1356369 (2024).

15. Hou, P. et al. Autophagy receptor CCDC50 tunes the STING-mediated interferon response in viral infections and autoimmune diseases. *Cell Mol. Immunol.* **18**, 2358–2371 (2021).
16. Liu, B. et al. Human STING is a proton channel. *Science* **381**, 508–514 (2023).
17. Saitoh, T. et al. Atg9a controls dsDNA-driven dynamic translocation of STING and the innate immune response. *Proc. Natl Acad. Sci. USA* **106**, 20842–20846 (2009).
18. Wan, W. et al. STING directly recruits WIPI2 for autophagosome formation during STING-induced autophagy. *EMBO J.* **42**, e112387 (2023).
19. Mizushima, N. & Komatsu, M. Autophagy: renovation of cells and tissues. *Cell* **147**, 728–741 (2011).
20. Kim, H. J., Lee, S. & Jung, J. U. When autophagy meets viruses: a double-edged sword with functions in defense and offense. *Semin Immunopathol.* **32**, 323–341 (2010).
21. Hait, A. S. et al. Defects in LC3B2 and ATG4A underlie HSV2 meningitis and reveal a critical role for autophagy in antiviral defense in humans. *Sci. Immunol*. **5** (2020).
22. O'Connell, D. & Liang, C. Autophagy interaction with herpes simplex virus type-1 infection. *Autophagy* **12**, 451–459 (2016).
23. Orvedahl, A. et al. HSV-1 ICP34.5 confers neurovirulence by targeting the Beclin 1 autophagy protein. *Cell Host Microbe* **1**, 23–35 (2007).
24. Giraldo, M. I., Hage, A., van Tol, S. & Rajsbaum, R. TRIM proteins in host defense and viral pathogenesis. *Curr. Clin. Microbiol. Rep.* **7**, 101–114 (2020).
25. Koepke, L., Gack, M. U. & Sparrer, K. M. The antiviral activities of TRIM proteins. *Curr. Opin. Microbiol*. **59**, 50–57 (2021).
26. van Gent, M., Sparrer, K. M. J. & Gack, M. U. TRIM proteins and their roles in antiviral host defenses. *Annu Rev. Virol.* **5**, 385–405 (2018).
27. Dutrieux, J. et al. PML/TRIM19-dependent inhibition of retroviral reverse-transcription by Daxx. *PLoS Pathog.* **11**, e1005280 (2015).
28. Ganser-Pornillos, B. K. & Pornillos, O. Restriction of HIV-1 and other retroviruses by TRIM5. *Nat. Rev. Microbiol*. **17**, 546–556 (2019).
29. Hoenigsperger, H. et al. CSNK2 suppresses autophagy by activating FLN-NHL-containing TRIM proteins. *Autophagy* **5**, 994–1014(2023).
30. Sparrer, K. M. J. et al. TRIM23 mediates virus-induced autophagy via activation of TBK1. *Nat. Microbiol*. **2**, 1543–1557 (2017).
31. Sparrer, K. M. J. & Gack, M. U. TRIM proteins: new players in virus-induced autophagy. *PLoS Pathog.* **14**, e1006787 (2018).
32. Chou, J., Kern, E. R., Whitley, R. J. & Roizman, B. Mapping of herpes simplex virus-1 neurovirulence to gamma 134.5, a gene nonessential for growth in culture. *Science* **250**, 1262–1266 (1990).
33. Yordy, B., Iijima, N., Huttner, A., Leib, D. & Iwasaki, A. A neuron-specific role for autophagy in antiviral defense against herpes simplex virus. *Cell Host Microbe* **12**, 334–345 (2012).
34. Meza-Carmen, V. et al. Regulation of growth factor receptor degradation by ADP-ribosylation factor domain protein (ARD) 1. *Proc. Natl Acad. Sci. USA* **108**, 10454–10459 (2011).
35. Leib, D. A., Alexander, D. E., Cox, D., Yin, J. & Ferguson, T. A. Interaction of ICP34.5 with Beclin 1 modulates herpes simplex virus type 1 pathogenesis through control of CD4+ T-cell responses. *J. Virol.* **83**, 12164–12171 (2009).
36. Bjorkoy, G. et al. p62/SQSTM1 forms protein aggregates degraded by autophagy and has a protective effect on huntingtin-induced cell death. *J. Cell Biol.* **171**, 603–614 (2005).
37. Klionsky, D. J. et al. Guidelines for the use and interpretation of assays for monitoring autophagy (4th edition)(1). *Autophagy* **17**, 1–382 (2021).
38. Arimoto, K. et al. Polyubiquitin conjugation to NEMO by triparite motif protein 23 (TRIM23) is critical in antiviral defense. *Proc. Natl Acad. Sci. USA* **107**, 15856–15861 (2010).
39. Laurent-Rolle, M. et al. The interferon signaling antagonist function of yellow fever virus NS5 protein is activated by type I interferon. *Cell Host Microbe* **16**, 314–327 (2014).
40. Gobeil, P. A. & Leib, D. A. Herpes simplex virus gamma34.5 interferes with autophagosome maturation and antigen presentation in dendritic cells. *mBio* **3**, e00267–00212 (2012).
41. Waisner, H. & Kalamvoki, M. The ICP0 Protein of Herpes Simplex Virus 1 (HSV-1) Downregulates Major Autophagy Adaptor Proteins Sequestosome 1 and Optineurin during the Early Stages of HSV-1 Infection. *J. Virol.* **93,** e01258–19 (2019).
42. Bjorkoy, G. et al. Monitoring autophagic degradation of p62/SQSTM1. *Methods Enzymol.* **452**, 181–197 (2009).
43. Dawidziak, D. M., Sanchez, J. G., Wagner, J. M., Ganser-Pornillos, B. K. & Pornillos, O. Structure and catalytic activation of the TRIM23 RING E3 ubiquitin ligase. *Proteins* **85**, 1957–1961 (2017).
44. Criollo, A. et al. The IKK complex contributes to the induction of autophagy. *EMBO J.* **29**, 619–631 (2010).
45. Lazarou, M. et al. The ubiquitin kinase PINK1 recruits autophagy receptors to induce mitophagy. *Nature* **524**, 309–314 (2015).
46. Michiorri, S. et al. The Parkinson-associated protein PINK1 interacts with Beclin1 and promotes autophagy. *Cell Death Differ.* **17**, 962–974 (2010).
47. Hiscott, J. Convergence of the NF-kappaB and IRF pathways in the regulation of the innate antiviral response. *Cytokine Growth Factor Rev.* **18**, 483–490 (2007).
48. Dempsey, A. & Bowie, A. G. Innate immune recognition of DNA: a recent history. *Virology* **479–480**, 146–152 (2015).
49. Hu, M. M. & Shu, H. B. Innate immune response to cytoplasmic DNA: mechanisms and diseases. *Annu Rev. Immunol.* **38**, 79–98 (2020).
50. Ma, Z., Ni, G. & Damania, B. Innate sensing of DNA virus genomes. *Annu Rev. Virol.* **5**, 341–362 (2018).
51. Sun, L., Wu, J., Du, F., Chen, X. & Chen, Z. J. Cyclic GMP-AMP synthase is a cytosolic DNA sensor that activates the type I interferon pathway. *Science* **339**, 786–791 (2013).
52. Chiang, J. J. et al. Viral unmasking of cellular 5S rRNA pseudogene transcripts induces RIG-I-mediated immunity. *Nat. Immunol.* **19**, 53–62 (2018).
53. Naesens, L. et al. GTF3A mutations predispose to herpes simplex encephalitis by disrupting biogenesis of the host-derived RIG-I ligand RNA5SP141. *Sci. Immunol.* **7**, eabq4531 (2022).
54. Zhang, S. Y. et al. TLR3 deficiency in patients with herpes simplex encephalitis. *Science* **317**, 1522–1527 (2007).
55. Lund, J., Sato, A., Akira, S., Medzhitov, R. & Iwasaki, A. Toll-like receptor 9-mediated recognition of Herpes simplex virus–2 by plasmacytoid dendritic cells. *J. Exp. Med*. **198**, 513–520 (2003).
56. Liu, D. et al. STING directly activates autophagy to tune the innate immune response. *Cell Death Differ.* **26**, 1735–1749 (2019).
57. Zhang, C. et al. Structural basis of STING binding with and phosphorylation by TBK1. *Nature* **567**, 394–398 (2019).
58. Herman, M. et al. Heterozygous TBK1 mutations impair TLR3 immunity and underlie herpes simplex encephalitis of childhood. *J. Exp. Med*. **209**, 1567–1582 (2012).
59. Ahmad, L. et al. Human TANK-binding kinase 1 is required for early autophagy induction upon herpes simplex virus 1 infection. *J. Allergy Clin. Immunol.* **143**, 765–769.e767 (2019).
60. Versteeg, G. A. et al. The E3-ligase TRIM family of proteins regulates signaling pathways triggered by innate immune pattern-recognition receptors. *Immunity* **38**, 384–398 (2013).
61. Di Rienzo, M., Romagnoli, A., Antonioli, M., Piacentini, M. & Fimia, G. M. TRIM proteins in autophagy: selective sensors in cell damage and innate immune responses. *Cell Death Differ.* **27**, 887–902 (2020).

62. Liang, Q. et al. Crosstalk between the cGAS DNA sensor and Beclin-1 autophagy protein shapes innate antimicrobial immune responses. *Cell Host Microbe* **15**, 228–238 (2014).
63. Lei, Y. et al. The mitochondrial proteins NLRX1 and TUFM form a complex that regulates type I interferon and autophagy. *Immunity* **36**, 933–946 (2012).
64. Heo, J. M., Ordureau, A., Paulo, J. A., Rinehart, J. & Harper, J. W. The PINK1-PARKIN Mitochondrial Ubiquitylation Pathway Drives a Program of OPTN/NDP52 Recruitment and TBK1 Activation to Promote Mitophagy. *Mol. Cell* **60**, 7–20 (2015).
65. Herhaus, L. et al. TBK1-mediated phosphorylation of LC3C and GABARAP-L2 controls autophagosome shedding by ATG4 protease. *EMBO Rep.* **21**, e48317 (2020).
66. Liyana, A. & Vanessa, S. S. The emerging role of human TBK1 in virus-induced autophagy. *Autophagy* **15**, 917–918 (2019).
67. Matsumoto, G., Shimogori, T., Hattori, N. & Nukina, N. TBK1 controls autophagosomal engulfment of polyubiquitinated mitochondria through p62/SQSTM1 phosphorylation. *Hum. Mol. Genet.* **24**, 4429–4442 (2015).
68. Richter, B. et al. Phosphorylation of OPTN by TBK1 enhances its binding to Ub chains and promotes selective autophagy of damaged mitochondria. *Proc. Natl Acad. Sci. USA* **113**, 4039–4044 (2016).
69. Vargas, J. N. S. et al. Spatiotemporal control of ULK1 Activation by NDP52 and TBK1 during Selective Autophagy. *Mol. Cell* **74**, 347–362.e346 (2019).
70. Weidberg, H. & Elazar, Z. TBK1 mediates crosstalk between the innate immune response and autophagy. *Sci. Signal* **4**, pe39 (2011).
71. Guo, B. & Cheng, G. Modulation of the interferon antiviral response by the TBK1/IKKi adaptor protein TANK. *J. Biol. Chem.* **282**, 11817–11826 (2007).
72. Marinho, F. V., Benmerzoug, S., Oliveira, S. C., Ryffel, B. & Quesniaux, V. F. J. The emerging roles of STING in bacterial infections. *Trends Microbiol.* **25**, 906–918 (2017).
73. Hong, C., Tijhuis, A. E. & Foijer, F. The cGAS Paradox: Contrasting Roles for cGAS-STING Pathway in Chromosomal Instability. *Cells* **8**, 1228 (2019).
74. Kim, J. et al. VDAC oligomers form mitochondrial pores to release mtDNA fragments and promote lupus-like disease. *Science* **366**, 1531–1536 (2019).
75. Sliter, D. A. et al. Parkin and PINK1 mitigate STING-induced inflammation. *Nature* **561**, 258–262 (2018).
76. Yu, C. H. et al. TDP-43 Triggers Mitochondrial DNA Release via mPTP to Activate cGAS/STING in ALS. *Cell* **183**, 636–649 e618 (2020).
77. Cadwell, K. Crosstalk between autophagy and inflammatory signalling pathways: balancing defence and homeostasis. *Nat. Rev. Immunol.* **16**, 661–675 (2016).
78. Delgado, M. A., Elmaoued, R. A., Davis, A. S., Kyei, G. & Deretic, V. Toll-like receptors control autophagy. *EMBO J.* **27**, 1110–1121 (2008).
79. Filomeni, G., De Zio, D. & Cecconi, F. Oxidative stress and autophagy: the clash between damage and metabolic needs. *Cell Death Differ.* **22**, 377–388 (2015).
80. Rodgers, M. A., Bowman, J. W., Liang, Q. & Jung, J. U. Regulation where autophagy intersects the inflammasome. *Antioxid. Redox Signal* **20**, 495–506 (2014).
81. Xun, J. et al. A conserved ion channel function of STING mediates noncanonical autophagy and cell death. *EMBO Rep.* **25**, 544–569 (2024).
82. Yamashiro, L. H. et al. Interferon-independent STING signaling promotes resistance to HSV-1 in vivo. *Nat. Commun.* **11**, 3382 (2020).
83. Zhu, J., Chiang, C. & Gack, M. U. Viral evasion of the interferon response at a glance. *J. Cell Sci.* **136,** jcs260682 (2023).
84. Pilli, M. et al. TBK-1 promotes autophagy-mediated antimicrobial defense by controlling autophagosome maturation. *Immunity* **37**, 223–234 (2012).
85. Liu, X., Matrenec, R., Gack, M. U. & He, B. Disassembly of the TRIM23-TBK1 complex by the Us11 protein of herpes simplex Virus 1 impairs autophagy. *J. Virol.* **93**, e00497–19. (2019).
86. Ma, Z. & Damania, B. The cGAS-STING defense pathway and its counteraction by viruses. *Cell Host Microbe* **19**, 150–158 (2016).
87. Ma, X. et al. Molecular basis of Tank-binding kinase 1 activation by transautophosphorylation. *Proc. Natl Acad. Sci. USA* **109**, 9378–9383 (2012).
88. Song, G. et al. E3 ubiquitin ligase RNF128 promotes innate antiviral immunity through K63-linked ubiquitination of TBK1. *Nat. Immunol.* **17**, 1342–1351 (2016).
89. Li, X. et al. Methyltransferase Dnmt3a upregulates HDAC9 to deacetylate the kinase TBK1 for activation of antiviral innate immunity. *Nat. Immunol.* **17**, 806–815 (2016).
90. Yu, J., Boyapati, A. & Rundell, K. Critical role for SV40 small-t antigen in human cell transformation. *Virology* **290**, 192–198 (2001).
91. Wies, E. et al. Dephosphorylation of the RNA sensors RIG-I and MDA5 by the phosphatase PP1 is essential for innate immune signaling. *Immunity* **38**, 437–449 (2013).
92. Parker, Z. M., Murphy, A. A. & Leib, D. A. Role of the DNA Sensor STING in Protection from Lethal Infection following Corneal and Intracerebral Challenge with Herpes Simplex Virus 1. *J. Virol.* **89**, 11080–11091 (2015).
93. Visser, L. J. et al. Dissecting distinct proteolytic activities of FMDV Lpro implicates cleavage and degradation of RLR signaling proteins, not its deISGylase/DUB activity, in type I interferon suppression. *PLoS Pathog.* **16**, e1008702 (2020).
94. Chiang, C., Dvorkin, S., Chiang, J. J., Potter, R. B. & Gack, M. U. The small t Antigen of JC virus antagonizes RIG-I-mediated innate immunity by inhibiting TRIM25's RNA binding ability. *mBio* **12**, e00620–21 (2021).
95. Chiang, C. et al. The Human Papillomavirus E6 Oncoprotein Targets USP15 and TRIM25 To Suppress RIG-I-Mediated Innate Immune Signaling. *J. Virol.* **92,** e01737–17 (2018).
96. Acharya, D. et al. Actin cytoskeleton remodeling primes RIG-I-like receptor activation. *Cell* **185**, 3588–3602.e3521 (2022).
97. Liu, G. et al. ISG15-dependent activation of the sensor MDA5 is antagonized by the SARS-CoV-2 papain-like protease to evade host innate immunity. *Nat. Microbiol* **6**, 467–478 (2021).
98. van Gent, M. et al. The US3 kinase of herpes simplex virus phosphorylates the RNA sensor RIG-I to suppress innate immunity. *J. Virol.* **96**, e0151021 (2022).
99. Serman, T. et al. Acetylation of the NS3 helicase by KAT5gamma is essential for flavivirus replication. *Cell Host Microbe* **31**, 1317–1330.e1310 (2023).
100. Volcic, M. et al. Vpu modulates DNA repair to suppress innate sensing and hyper-integration of HIV-1. *Nat. Microbiol.* **5**, 1247–1261 (2020).
101. Xue, Y. et al. GPS: a comprehensive www server for phosphorylation sites prediction. *Nucleic Acids Res* **33**, W184–W187 (2005).
102. Zou, L. et al. PKIS: computational identification of protein kinases for experimentally discovered protein phosphorylation sites. *BMC Bioinforma.* **14**, 247 (2013).

Acknowledgements

We greatly thank M. Vaughan (NIH), D. Leib (Dartmouth University) and M. Diamond (WUSTL) for providing key reagents. We thank Jana-Romana Fischer and Birgit Ott for their excellent technical support. We are also

grateful to Cindy Chiang for support with MS data visualization. This work was supported by the U.S. National Institutes of Health grants R01 AI148534 and AI087846 (to M.U.G.) and the German Research Foundation grants CRC 1279, SPP 1923, SP 1600/7-1 and SP 1600/9-1 (to K.M.J.S.). K.M.J.S. is also supported by the German Ministry for Education and Research (BMBF; project IMMUNOMOD 01KI2014). M.H. is supported by the "Baustein" program of Ulm University Medical Faculty (project number L.S.B.N.0245). H.H. is part of the International Graduate School for Molecular Medicine at Ulm University (IGradU). J.K. and J.M. were supported by the Division of Intramural Research, National Institutes of Health, National Heart, Lung, and Blood Institute.

Author contributions

M.U.G. conceived and designed the study; D.A., Z.S., H.H., M.H., M.Z., K.B., J.Z. and S.G. performed the experiments and analyzed the data; D.A. and M.U.G. wrote the primary manuscript draft; D.A., K.M.J.S. and M.U.G. reviewed and edited the manuscript; K.M.J.S. and M.U.G. secured the funding; S.-Y.Z., J.-L.C., J.K. and J.M. provided critical resources; K.M.J.S. and M.U.G. supervised the study. All authors reviewed the manuscript prior to submission.

Competing interests

The authors declare no competing interests.

Additional information

Supplementary information The online version contains supplementary material available at https://doi.org/10.1038/s41467-025-59338-5.

Correspondence and requests for materials should be addressed to Michaela U. Gack.

Peer review information *Nature Communications* thanks the anonymous reviewer(s) for their contribution to the peer review of this work. A peer review file is available.